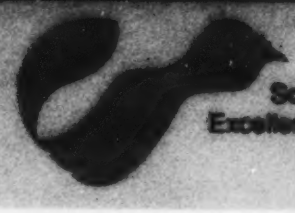

Scientific Excellence • Resource Protection & Conservation • Benefits for Canadians
Excellence scientifique • Protection et conservation des ressources • Bénéfices aux Canadiens

Near-Surface Moored Current Meter Intercomparisons

by
M.J. Woodward,
W.S. Huggett
and
R.E. Thomson

Institute of Ocean Sciences
Department of Fisheries and Oceans
Sidney, B.C.

1990

Canadian Technical Report of Hydrography and Ocean Sciences No. 125

Canadian Technical Report of Hydrography and Ocean Sciences

Technical reports contain scientific and technical information that contributes to existing knowledge but which is not normally appropriate for primary literature. The subject matter is related generally to programs and interests of the Ocean Science and Surveys (OSS) sector of the Department of Fisheries and Oceans.

Technical reports may be cited as full publications. The correct citation appears above the abstract of each report. Each report is abstracted in *Aquatic Sciences and Fisheries Abstracts* and indexed in the Department's annual index to scientific and technical publications.

Technical reports are produced regionally but are numbered nationally. Requests for individual reports will be filled by the issuing establishment listed on the front cover and title page. Out of stock reports will be supplied for a fee by commercial agents.

Regional and headquarters establishments of Ocean Science and Surveys ceased publication of their various report series as of December 1981. A complete listing of these publications is published in the *Canadian Journal of Fisheries and Aquatic Sciences*, Volume 39: Index to Publications 1982. The current series, which begins with report number 1, was initiated in January 1982.

Rapport technique canadien sur l'hydrographie et les sciences océaniques

Les rapports techniques contiennent des renseignements scientifiques et techniques qui constituent une contribution aux connaissances actuelles, mais qui ne sont pas normalement appropriés pour la publication dans un journal scientifique. Le sujet est généralement lié aux programmes et intérêts du service des Sciences et levés océaniques (SLO) du ministère des Pêches et des Océans.

Les rapports techniques peuvent être cités comme des publications complètes. Le titre exact paraît au-dessus du résumé de chaque rapport. Les rapports techniques sont résumés dans la revue *Résumés des sciences aquatiques et halieutiques*, et ils sont classés dans l'index annuel des publications scientifiques et techniques du Ministère.

Les rapports techniques sont produits à l'échelon régional, mais numérotés à l'échelon national. Les demandes de rapports seront satisfaites par l'établissement auteur dont le nom figure sur la couverture et la page du titre. Les rapports épuisés seront fournis contre rétribution par des agents commerciaux.

Les établissements des Sciences et levés océaniques dans les régions et à l'administration centrale ont cessé de publier leurs diverses séries de rapports en décembre 1981. Une liste complète de ces publications figure dans le volume 39, Index des publications 1982 du *Journal canadien des sciences halieutiques et aquatiques*. La série actuelle a commencé avec la publication du rapport numéro 1 en janvier 1982.

Canadian Technical Report of
Hydrography and Ocean Sciences
No. 125

1990

NEAR-SURFACE MOORED CURRENT METER INTERCOMPARISONS

by

M.J. Woodward, W.S. Huggett and R.E. Thomson

Institute of Ocean Sciences
Department of Fisheries and Oceans
Sidney, B.C.

91-01832/

Copyright Minister of Supply and Services Canada - 1990
Cat. No. Fs 97-18/125 ISSN 0711-6764

Correct Citation for this report is:

Woodward, M.J., W.S. Huggett and R.E. Thomson. 1990. Near-Surface Moored Current Meter Intercomparisons. Can. Tech. Rep. Hydrogr. Ocean Sci. No. 125: 65 pp.

CONTENTS

ABSTRACT..... ix
RESUME..... x

1. INTRODUCTION..... 1

2. CURRENT METER CHARACTERISTICS..... 3
   2.1 Aanderaa RCM4..... 3
   2.2 Dumas Neyrpic model CMDR modified by Applied Microsystems Ltd..... 3
   2.3 EG&G VMCM model 630..... 3
   2.4 Endeco type 174..... 4
   2.5 Geodyne 850 modified by Applied Microsystems Ltd..... 4
   2.6 Neil Brown ACM2..... 4
   2.7 Marsh-McBirney 585..... 4
   2.8 Sea Data 620..... 5
   2.9 Simrad UCM model 37..... 5

3. THE THREE GROUPS OF EXPERIMENTAL MOORINGS..... 5
   3.1 Mooring Elements..... 5
   3.2 Queen Charlotte Sound..... 6
   3.3 Strait of Georgia..... 6
   3.4 Hecate Strait..... 8

4. CURRENT METER PREPARATION AND CALIBRATION..... 10

5. CURRENT METER PERFORMANCE AT EACH SITE..... 10
   5.1 Queen Charlotte Sound..... 10
   5.2 Strait of Georgia..... 12
   5.3 Hecate Strait..... 22

6. SUMMARY OF CURRENT METER PERFORMANCE..... 28
   6.1 Aanderaa RCM4 with Savonius-like rotor..... 28
   6.2 Aanderaa RCM4 with paddle-wheel rotor..... 28
   6.3 Dumas Neyrpic model CMDR modified by Applied Microsystems Ltd..... 29
   6.4 EG&G VMCM model 630..... 29
   6.5 Endeco type 174..... 29
   6.6 Geodyne 850 modified by Applied Microsystems Ltd..... 30
   6.7 Marsh-McBirney 585..... 30
   6.8 Neil Brown ACM2..... 31
   6.9 Sea Data 620..... 31
   6.10 Simrad UCM model 37..... 31

7. CONCLUSIONS..... 31

8. ACKNOWLEDGEMENTS..... 32

9. REFERENCES..... 33
TABLES..... 35
FIGURES..... 41

LIST OF FIGURES

Figure 1. General locations of the three mooring groups..... xii

Figure 2. Sites of experimental moorings in Queen Charlotte Sound..... 7

Figure 3. Sites of experimental moorings in the Strait of Georgia..... 7

Figure 4. Sites of experimental moorings in Hecate Strait..... 9

Figure 5. Moorings in Queen Charlotte Sound..... 43

Figure 6. Moorings in the Strait of Georgia..... 44

Figure 7. Moorings in Hecate Strait..... 45

Figure 8. Time series plots of unfiltered current measurements from Queen Charlotte Sound..... 46

Figure 9. Scatter diagrams of speed between current meters and histograms of the occurrence of speed for Queen Charlotte Sound. The bold trace in each histogram corresponds to the speeds plotted on the horizontal axis of the attached scatter diagram..... 47

Figure 10. Power spectra of current measurements in Queen Charlotte Sound..... 48

Figure 11. Time series plots of unfiltered current measurements from the surface-following mooring GMA for the period October 15-17 in the Strait of Georgia..... 49

Figure 12. Time series plots of unfiltered current measurements from the surface-following mooring GMA for the period October 25-27 in the Strait of Georgia..... 50

Figure 13. Scatter diagrams of speed between current meters and histograms of the occurrence of speed for the surface-following mooring GMA in the Strait of Georgia. The bold trace in each histogram corresponds to the speeds plotted on the horizontal axis of the attached scatter diagram..... 51

Figure 14. Power spectra of current measurements for the surface-following mooring GMA in the Strait of Georgia..... 52

Figure 15. Time series plots of unfiltered current measurements from the surface-following mooring GMB in the Strait of Georgia..... 53

Figure 16. Scatter diagrams of speed between current meters and histograms of the occurrence of speed for the surface-following mooring GMB in the Strait of Georgia. The bold trace in each histogram corresponds to the speeds plotted on the horizontal axis of the attached scatter diagram..... 54

Figure 17. Power spectra of current measurements for the surface-following mooring GMB in the Strait of Georgia..... 55

Figure 18. Time series plots of unfiltered current measurements from the instruments at 50m on the subsurface mooring GSW in the Strait of Georgia..... 56

Figure 19. Scatter diagrams of speed between current meters and histograms of the occurrence of speed for the instruments at 50m on the subsurface mooring GSW in the Strait of Georgia. The bold trace in each histogram corresponds to the speeds plotted on the horizontal axis of the attached scatter diagram..... 57

Figure 20. Power spectra of currents as measured by the Aanderaa RCM4 (Savonius-like) and Geodyne-AML instruments at 50m on the subsurface mooring GSW in the Strait of Georgia..... 58

Figure 21. Time series plots of unfiltered current measurements from the instruments at 50m and 100m on the subsurface mooring GNE in the Strait of Georgia..... 59

Figure 22. Scatter diagrams of speed between current meters and histograms of the occurrence of speed for the instruments at 50m and 100m on the subsurface mooring GNE in the Strait of Georgia. The bold trace in each histogram corresponds to the speeds plotted on the horizontal axis of the attached scatter diagram..... 60

Figure 23. Time series plots of current as measured by Marsh-McBirney 585's on surface-following and subsurface moorings, W05 and W5S, in Hecate Strait..... 61

Figure 24. Time series plots of unfiltered current measurements from the subsurface mooring W05 in Hecate Strait..... 62

Figure 25. Scatter diagrams of speed between current meters and histograms of the occurrence of speed for Hecate Strait. The bold trace in each histogram corresponds to the speeds plotted on the horizontal axis of the attached scatter diagram..... 63

Figure 26. Power spectra of currents as measured by Marsh-McBirney 585's on surface-following and subsurface moorings, W05 and W5S, in Hecate Strait..... 64

Figure 27. Power spectra of current measurements from the subsurface mooring W05 in Hecate Strait..... 65

LIST OF TABLES

TABLE 1. Characteristics of current meters with mechanical speed sensors..... 37

TABLE 2. Characteristics of current meters with electromagnetic or acoustic speed sensors..... 38

TABLE 3. Current meter deployment details..... 39

ABSTRACT

Woodward, M.J., W.S. Huggett and R.E. Thomson. 1990. Near-Surface Moored Current Meter Intercomparisons. Can. Tech. Rep. Hydrogr. Ocean Sci. No. 125: 65 pp.

Three experiments to evaluate the performance of near-surface moored current meters were conducted over the period May 1982 to September 1983 at sites in coastal waters of western Canada. The instrument types used were the standard Aanderaa RCM4 plus one RCM4 fitted with an experimental paddle-wheel rotor, the Geodyne 850 modified by Applied Microsystems Ltd. to record one sample per second, the Dumas Neyrpic model CMDR modified for recording on magnetic tape, the Endeco type 174, the EG&G VMCM model 630, the Marsh-McBirney 585, the Neil Brown ACM2, the Sea Data 620 and the Simrad UCM model 37. The current meters were deployed within 10 metres of the surface except for two deeper subsurface moorings with instruments at 50 and 100 metres.

Results show that the instruments suspended from surface floats were commonly operating in environments with *noise-to-signal* ratio (wave-induced to mean current) values in the range of two to five. The instruments moored near the surface showed large differences in performance which are attributed to the varying ability of the sensor and sampling scheme combinations to measure or reject surface-wave-induced noise. Only the EG&G VMCM model 630 and the Marsh-McBirney 585 appeared to be capable of handling the noise levels associated with a surface mooring in the presence of a moderate wave field, but our testing of the Sea Data 620 was inconclusive. Our results in the wave zone for the Aanderaa RCM4 with Savonius-like rotor are consistent with the error predictions of Hammond *et al.* (1986) and cast serious doubt on the conclusions of Pearson *et al.* (1981). The data from all instruments moored with subsurface floatation at 50 metres depth agreed very well, both in speed and direction; typical values were within two centimetres per second and five degrees.

Keywords: current measurement, current meter, intercomparison, near-surface.

RESUME

Woodward, M.J., W.S. Huggett and R.E. Thomson. 1990. Near-Surface Moored Current Meter Intercomparisons. Can. Tech. Rep. Hydrogr. Ocean Sci. No. 125: 65 pp.

Trois expériences visant à évaluer des courantomètres amarrés près de la surface ont été réalisés de mai 1982 à septembre 1983 dans les eaux côtières de l'ouest Canadien. Les types d'instrument employés furent le Aanderaa RCM4 standard avec un RCM4 équipé d'une roue à palettes, le Geodyne 850 modifié par Applied Microsystems S.A. pour enregistrer un échantillon par seconde, le Dumas Neyrpic modèle CMDR modifié pour l'enregistrement sur bande magnétique, l'Endeco modèle 174, l'EG&G VMCM modèle 630, le Marsh-McBirney 585, le Neil Brown ACM2, le Sea Data 620 et le Simrad UCM modèle 37. Les courantomètres ont été mis en place à moins de 10 mètres de la surface à l'exception de deux amarrages plus profonds avec des instruments à 50 et à 100 metres.

Les résultats indiquent que les instruments fixés sous une bouée fonctionnaient normalement dans des milieux avec des rapports bruit-signal (vagues versus courant moyen) valeurs de 2 à 5. Les instruments fixés à une faible profondeur sous une bouée ont révélé de grandes différences de rendement ce qui peut être attribué à l'habileté variable du capteur et des combinaisons des techniques d'échantillonage à mesurer ou rejeter le bruit produit par les vagues de la surface. Il n'y a que l'EG&G VMCM modèle 630 et le Marsh-McBirney 585 qui apparemment étaient capable de bien fonctionner avec les niveaux de bruit associés à un amarrage près de la surface en présence d'un champ de vagues moyennes, mais nos essais du Sea Data 620 ont été peu concluants. Nos résultats dans la zone de vagues en ce qui concerne le Aanderaa RCM4 avec le rotor tel que le Savonius sont en accord avec les prédictions des erreurs de Hammond et al. (1986), et ils émettent des doutes sur les conclusions de Pearson et al. (1981). Les données de tous les instruments mis à flot à 50 metres sous la surface concordèrent très bien, pour la vitesse aussi bien que pour la direction, des valeurs caractéristiques furent à 2 cm/s et dégres près.

Mots-clés: Mesures des courants, courantomètre, essai comparatif, près de la surface.

INTENTIONALLY BLANK

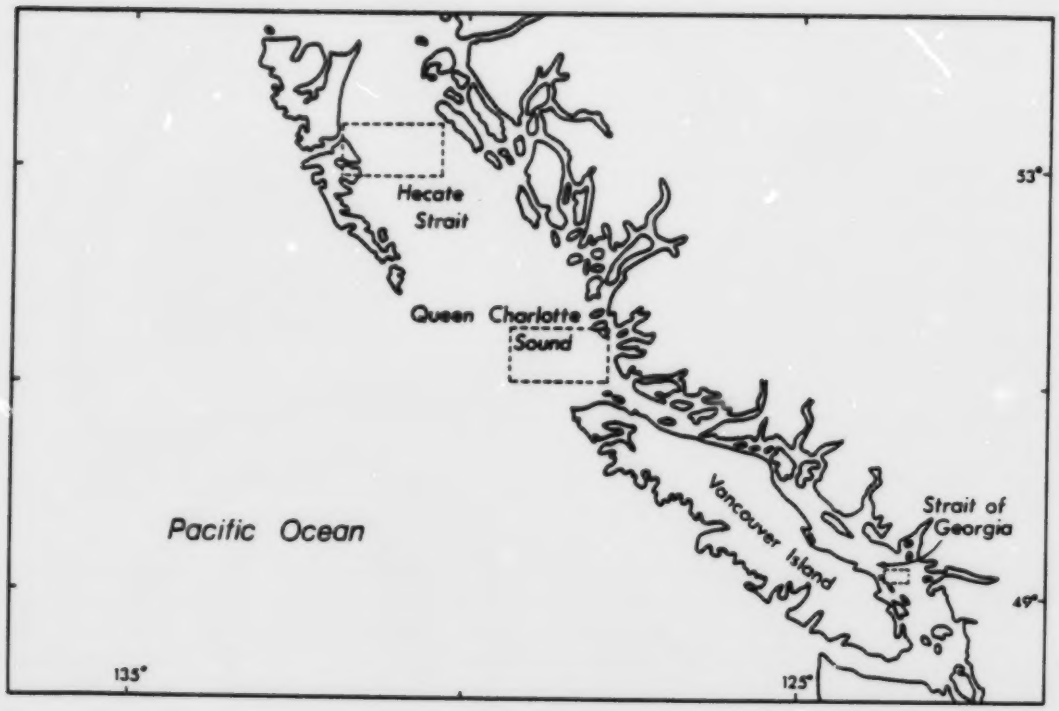

Figure 1. General locations of the three mooring groups.

1. INTRODUCTION

To evaluate the performance in the near-surface environment of several recently introduced current meters along with well-established ones, three groups of experimental moorings were installed over various periods between May 1982 and September 1983. The general locations of the three sites in the coastal waters of western Canada are shown in Figure 1. Ten different instrument types were compared with a total of twenty-three instruments deployed on five surface and six subsurface moorings.

The emphasis in these experiments was on comparison of instruments mounted as close together as possible on the same mooring. This arrangement avoids the difficulty of verifying that an identical current occurred at two separate moorings. While it must be recognised that the characteristics of a mooring can significantly affect current meter performance, especially in the case of surface moorings, the moorings for these experiments were not optimised to suit a particular instrument, except in the case of the Endeco type 174. In the situation where a current meter is strongly under the influence of a surface gravity wave field, the interaction between the waves and the combined system of the current meter and its mooring are complex and will be touched upon only briefly here.

A number of investigators have examined the quality of measurements obtained by current meters carried by surface and/or subsurface moorings. Among them Halpern *et al.* (1974), Saunders (1976), Beardsley *et al.* (1981), Kuhn *et al.* (1980), Pearson *et al.* (1981), and Hammond *et al.* (1986). The direct and indirect effects of surface-wave-induced motions are generally accepted as the main cause of current meter error in near-surface applications.

No attempt is made here to separate the direct effects of the surface-wave-induced fluctuations in the current from the indirect effects of the interaction of the surface waves with the mooring. Wherever possible, estimates have been made of the noise, which we define for the purposes of further discussion to be the combined direct and indirect surface-wave-frequency fluctuations in the current as seen by the current meter. In some cases measurements of these fluctuations were made by rapid sampling of the current while in others the direct effect of the surface wave action was computed from wave measurements. In other cases, a qualitative estimate of the wave conditions was inferred from local meteorological data. These estimates of the

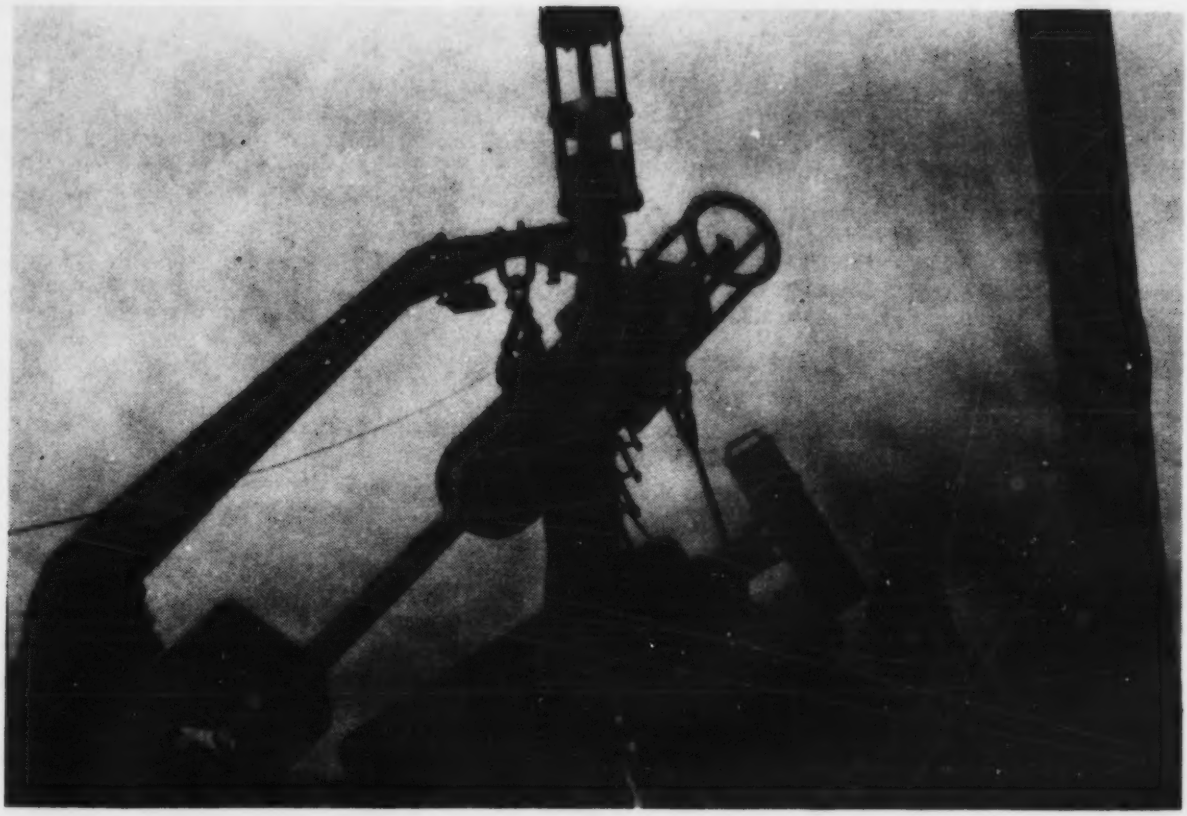

Plate 1. The cluster of three current meters at the top of mooring GSW.

amplitude of the noise are compared with the measurements made by two closely spaced current meters to obtain a measure of their relative performance in various conditions of current and signal-to-noise ratio.

2. CURRENT METER CHARACTERISTICS

The characteristics of the current meters which were evaluated in this experiment are summarised in Tables 1 and 2. The grouping of the instruments in these tables is not intended to indicate any preference for mechanical sensor types as opposed to those with no moving parts.

2.1 Aanderaa RCM4

The Aanderaa RCM4 is perhaps the most successful instrument in oceanographic current measurement if the number of instruments in service since their introduction in June 1966 is taken as a measure of success. This instrument records a sum of rotor revolutions at regular intervals along with an instantaneous sample of direction. The original rotor is similar to a Savonius rotor. A paddle wheel rotor, available as of 1983, gives a much improved performance in the wave zone. For further details see Unesco (1970), Beardsley *et al.* (1981) and Hammond *et al.* (1986).

2.2 Dumas Neyrpic model CMDR modified by Applied Microsystems Ltd.

The Dumas Neyrpic CMDR originally recorded on punched paper tape. The modification by Applied Microsystems was by way of an updated controller, compass and recorder. The sampling scheme is identical with the Aanderaa RCM4, but the mechanical configuration is entirely different. The axis of rotation of the propeller is horizontal, coaxial with the pressure case and the direction vane support shaft, as may be seen in the center of Plate 1. The propeller is protected by a ring supported on four rods projecting from the periphery of the forward part of the pressure case.

2.3 EG&G VMCM model 630

The VMCM carries two orthogonal rotors which are designed to have cosine response to angle of attack, so that the rotors sense the horizontal components of velocity with respect to the instrument case. These components are transformed into East and North components on-board the instrument and only the vector average is recorded. For further details see Weller and Davis (1980).

2.4 Endeco type 174

The Endeco current meter is unusual in that it is not connected directly to the mooring line, but is tethered by several metres of 10 mm rope to a swiveling attachment point. The unit must be ballasted to make it neutrally buoyant. A large diameter propeller is mounted axially with the pressure case on the tail end of the unit and is enclosed in a duct which also serves as the direction vane. The purpose of the flexible attachment is to allow the instrument to follow fluctuations in the flow - particularly in the vertical - and so prevent much of this motion from affecting the rotor. The sampling scheme is identical with that of the Aanderaa RCM4.

2.5 Geodyne 850 modified by Applied Microsystems Ltd.

The Geodyne 850 is the predecessor of the EG&G VACM with virtually identical sensors consisting of a caged Savonius rotor and small caged vane. The sensors are mounted on the lower end of the pressure case which appears in the upper center of Plate 1. The modifications made by Applied Microsystems incorporated a 9-track 1600 BPI recorder so that bursts at one second intervals are practical. The original sensors are used with the exception of the fitting of a replacement compass and vane follower manufactured by Digicourse. For details of the original Geodyne 850 see Beardsley *et al.* (1981).

2.6 Neil Brown ACM2

The Neil Brown current meter operates using differences in acoustic travel time and continuously measures the horizontal components of velocity with respect to the instrument case. These measurements are transformed by an analogue computer into East and North components which are accumulated and stored at regular intervals. The sensors are mounted on the lower end of the pressure case in close proximity to the end plate. The mirror support structure and the pressure case can easily generate wakes which intersect the active measurement volume, particularly in the presence of vertical motion.

2.7 Marsh-McBirney 585

The Marsh-McBirney 585 operates on the principle of the generation of an electric field by the motion of a conductor (the flow of water) through a magnetic field. An alternating magnetic field is produced by an electromagnet within the spherical sensor and the two horizontal components of the electric field are detected by two pairs

of orthogonal electrodes. The resulting components of velocity are vector-averaged on board the instrument before being recorded.

2.8 Sea Data 620

The Sea Data instrument employs a sensor identical with that of the Marsh-McBirney 585 but does not perform vector averages on board. The sampling scheme is of bursts of measurements which result from filtering the sensor output with a filter time constant corresponding to the sample rate within each burst. The units have such storage capacity that relatively long bursts may be recorded without endurance problems.

2.9 Simrad UCM model 37

The Simrad UCM employs sensors very similar to the Neil Brown ACM2, but the sensors are more remote from the pressure case and are more streamlined to reduce the problem of wakes interfering with the measurement process. This instrument does not incorporate any vector averaging capability which limits the endurance if high sample rates are required.

3. THE THREE GROUPS OF EXPERIMENTAL MOORINGS

3.1 Mooring Elements

The surface floats for these experimental moorings, excepting G5A, consisted of a 2.2 m diameter toroid with a 3.5 m tower carrying meteorological sensors and a 1.8 m tripod beneath the toroid connecting the float to the mooring line. These were moored by a single taught line to the bottom where a ballast of heavy chain provided the mooring tension.

The main subsurface floats were of aluminum, formed of two partial hemispheres with a stabilising fin. The net buoyancy of these floats is approximately 3900 N with a frontal area of 0.62 m^2. This design of float helps to minimise the mooring motion associated with vortex shedding, which can be a problem when spherical floats are used. The subsurface moorings were all of single-point design, main floatation being provided by the floats described above and using back-up floatation within 5 m of the bottom. Except where specifically stated, the mooring lines for the

subsurface moorings were of 6 mm galvanised steel wire rope with 1 m sections of 20 mm synthetic rope used as isolation links. The depths of the subsurface moorings shown in the mooring configuration figures are depths below the level of the lowest predictable tide.

3.2 Queen Charlotte Sound

The two moorings in Queen Charlotte Sound were deployed near 51° 21'N, 128° 53'W in 240 m of water and were separated by approximately 1 km. These were in position from May 28 to September 16, 1982. It may be seen in Figure 2 that the moorings were placed in the middle of a reentrant trough which deepens to the west and continues out to the continental shelf break. The mooring site was exposed to Pacific swell from the west.

The mooring configurations are shown in Figure 5. Mooring G5S carried a single EG&G VMCM 5 m below the surface and a 25 mm synthetic mooring line connected this instrument to the chain ballast which maintained approximately 3900 N of tension. A Marsh-McBirney 585 was to be deployed with the VMCM but the unit developed a fault at sea which could not be repaired in time for deployment.

Mooring G5A carried a Geodyne 850 immediately above a Dumas Neyrpic model CMDR at a depth of 10 m below mean sea level. The tidal range in the area is approximately 4 m and the top of the subsurface float was 6 m below mean sea level. A light surface mooring was attached to the top of this subsurface float with an Endeco type 174 tethered 5 m below the surface. This mooring consisted of a 60 cm diameter bladder from which a 20 kg counterweight was suspended with 7 m of 15 mm nylon line, which was in turn connected to the top of the subsurface float with a further 12 m of Nylon line. A small float was attached to the 12 m line at a point 3 m above the subsurface float to help keep this line from becoming tangled around the subsurface float.

3.3 Strait of Georgia

In the Strait of Georgia, two subsurface moorings were deployed during the period October 14 to December 8, 1982 around a central surface mooring near 49° 11'N, 123° 30'W, in 340 m of water (cf. Figure 3). The longest fetch is approximately 60 km from a southeasterly direction, the usual direction of winter storm winds.

The central surface mooring carried two successive strings of current meters near the surface. The first of these two instrument strings was removed from the mooring on November

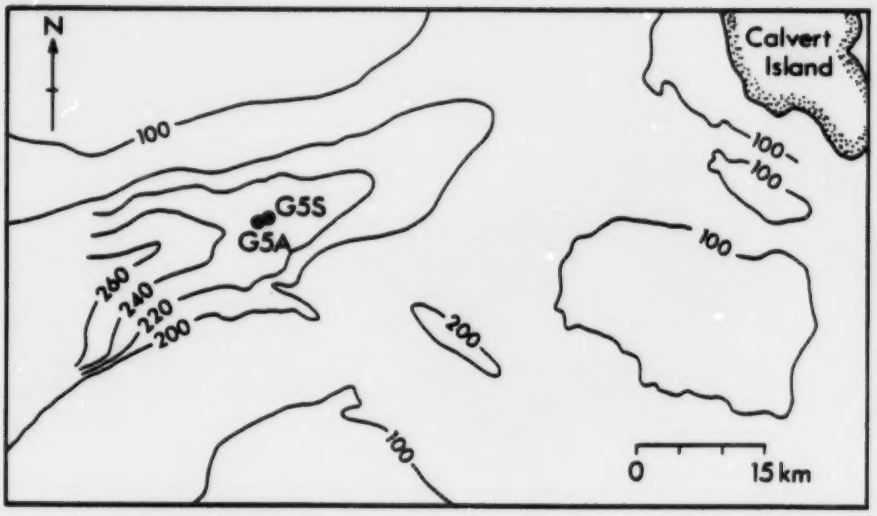

Figure 2. Sites of experimental moorings in Queen Charlotte Sound.

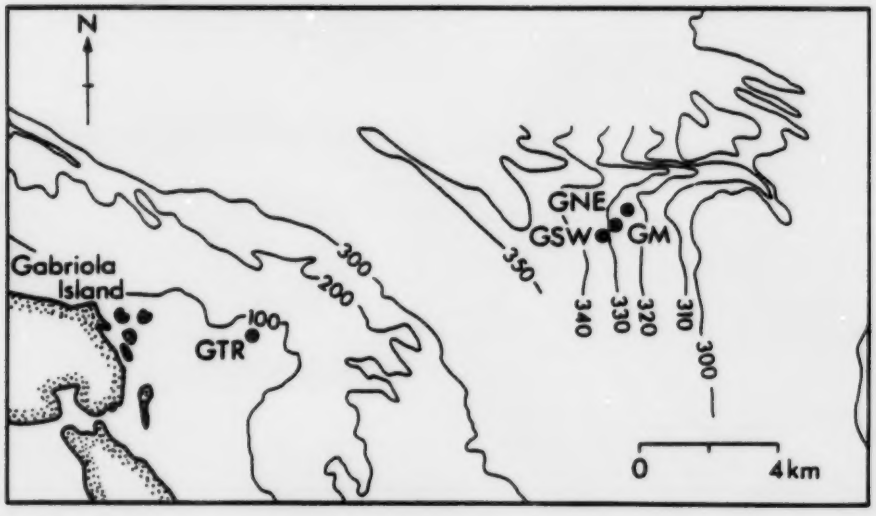

Figure 3. Sites of experimental moorings in the Strait of Georgia.

2 and replaced by the second set of instruments. The first deployment, in Figure 6, designated GMA, consisted of a Geodyne 850 mounted immediately above a Marsh-McBirney 585 which was connected directly to an EG&G VMCM. The second deployment, designated GMB, consisted of a Neil Brown ACM2 connected to a Marsh-McBirney 585 in inverted mode below which were a Sea Data 620 and a Simrad UCM model 37. The mooring hardware was identical in both of these deployments with a mooring line of 25 mm synthetic rope and a chain ballast maintaining nominally 2900 N of mooring tension above the back-up floatation. Wind speed and direction were measured by a J-TEC vortex-shedding anemometer mounted 4 m above the sea surface and interfaced to an AML datalogger. Moorings GSW and GNE were both deployed approximately 500 m from this central mooring.

The instrument configuration on mooring GSW at 50 m consisted of a Geodyne 850 a Dumas Neyrpic model CMDR, and an Aanderaa RCM4 (cf. Plate 1) connected directly together such that the sensors spanned less than 1 m in the vertical.

Mooring GNE was deployed on November 2 at the time of the exchange of instruments on the central mooring. At 50 m depth a Geodyne 850 was connected directly to a Neil Brown ACM2 in inverted mode, resulting in a vertical sensor spacing of 60 cm. At 100 m a standard Aanderaa RCM4 was placed together with an RCM4 fitted with an experimental paddle-wheel rotor and semi-circular shield.

3.4 Hecate Strait

Two moorings were deployed in Hecate Strait near 53° 11'N, 131° 17'W in 40 m of water over the period May 14 to September 20, 1983 (cf. Figure 4). This site is on Dogfish Bank, a relatively flat bank approximately 40 km in width extending 60 km to the south of the moorings and to the northern extremity of the Queen Charlotte Islands. There is protection from Pacific swell except from the south. The fetch to the southeast, the predominant direction of storm winds, is restricted to 300 km by the northern end of Vancouver Island. The configurations of the moorings in Hecate Strait are shown in Figure 7.

On the surface mooring W5S, a Marsh-McBirney 585 current meter was deployed at a depth of 5 m. Wind speed was measured 4 m above the surface using a J-TEC vortex-shedding anemometer interfaced to an AML recorder. The mooring line consisted of 30 mm anchor chain maintaining nominally 3900 N of tension and with isolation links of 25 mm synthetic rope above and below the current meter.

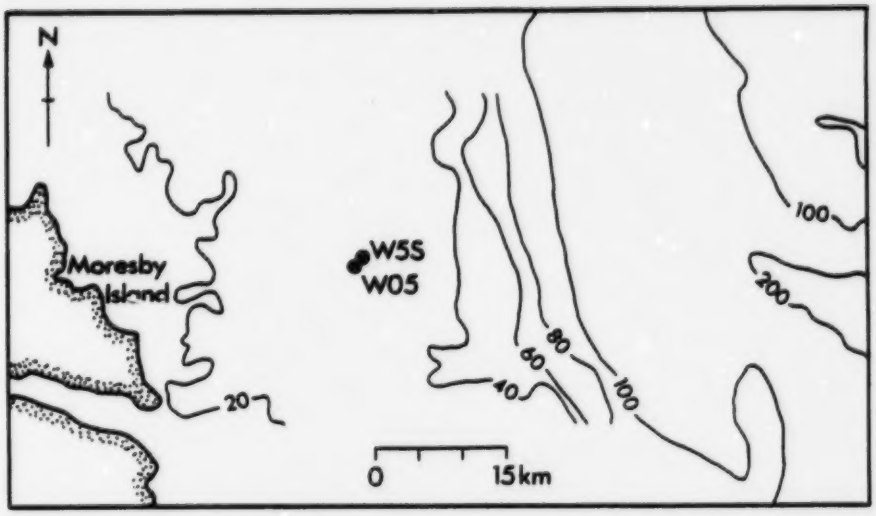

Figure 4. Sites of experimental moorings in Hecate Strait.

The subsurface mooring, designated W05, carried a Marsh-McBirney 585 above an Aanderaa RCM4 fitted with an experimental paddle-wheel rotor and a standard Aanderaa RCM4. These three instruments were connected directly together resulting in a vertical sensor span of 1.3 m. The subsurface float was 1 m above the upper instrument and the mooring line was of 20 mm synthetic rope. The two pressure recorders were mounted in break-away fixtures in the concrete anchor.

4. CURRENT METER PREPARATION AND CALIBRATION

Preparation of the instruments was done by staff at the Institute of Ocean Sciences (IOS) in accordance with the manufacturer's instructions, except as indicated in the acknowledgements.

The Marsh-McBirney 585's were calibrated by the manufacturer before and after the experiment and showed no measurable change in calibration (less than a few mm/sec). The other manufacturer's calibrations were accepted as correct, with the exception of the Aanderaa RCM4's which had compass calibrations done at IOS.

5. CURRENT METER PERFORMANCE AT EACH SITE

5.1 Queen Charlotte Sound

Several equipment failures in this first experiment resulted in considerable loss of data. The Marsh-McBirney 585, which was to be placed together with the EG&G VMCM on mooring G5S, developed a fault which was not repaired in time for deployment. The Geodyne on mooring G5A and the Aanderaa wind speed sensor mounted on the surface float of mooring G5S both failed during deployment. In addition to these problems, after six weeks or so a discarded length of 15 mm manilla rope became entangled in the propellers of the VMCM. This tendency of these five-bladed propellers to become entangled may be a strong consideration in some applications, though there is some protection of the propellers by the instrument cage.

The loss of the wind speed sensor means that we have no qualitative indicator of the wave conditions, although a general statement can be made regarding typical wave conditions for the season. There is almost always swell with periods in the vicinity of 10 seconds and a typical amplitude of 1 m reaching this site from the Pacific. Linear wave theory predicts that such waves would result in

an average horizontal fluctuation in the current of 50 cm/sec at 5 m and 40 cm/sec at 10 m. Waves generated by local winds are of shorter period than these, usually 3 to 7 seconds. Winds in the summer months are generally light, so the differences seen here would certainly be greater in conditions more typical of the seasonal average, and much greater in winter storm conditions.

A typical segment of the time series of currents from moorings G5A and G5S is shown in Figure 8, repeating the data from the CMDR as a common reference. The data used in these time series plots were not filtered and are presented at the original sample interval. For the scattergrams of speed versus speed and the histograms of the occurrence of a particular speed, shown in Figure 9, the data were filtered by a three-pass moving-average filter one hour in length, then subsampled to hourly values. The period of data taken for Figure 9 and for the spectra in Figure 10 is given under "duration" in Table 3, a total length of 2048 hours.

The time series plots of the currents recorded by the Endeco and CMDR instruments show similar velocities, but the Endeco consistently measures a higher speed. This was not unexpected as the Endeco was suspended from a surface float and so was exposed to larger wave-induced fluctuations than was the CMDR, which was on a subsurface mooring and had a relatively more stable reference frame. The sampling scheme is virtually identical for both of these instruments, a continuous accumulation of rotor count which is sampled at regular intervals along with an instantaneous measurement of direction. The main difference between them is their type of attachment to the mooring line. The CMDR is inserted into the mooring line while the Endeco is tethered to the mooring line by a 1.5 m synthetic rope (cf. Figure 5). This tether, which was supplied by Endeco, isolates the instrument from much of the wave-induced fluctuation in the current by allowing the instrument, which is neutrally buoyant, to move with fluctuations in the mean flow. That the agreement is as good as it is despite the substantial difference in the noise that each instrument measures is a plus for the capability of the Endeco, which is relatively inexpensive compared with vector averaging current meters.

The speed scatter diagram and histogram in the upper left of Figure 9 also reflect the consistently high speed measured by the Endeco when mounted beneath a surface float and exposed to ocean swell, but over a longer period - 2048 hours. At higher speed, the speed histograms show a tendency to converge due to the improved signal-to-noise ratio. The power spectra shown in Figure 10 were computed using the same data as for the scatter plots and the

histograms. The Endeco measures consistently higher speeds and there is indication of better agreement at tidal frequencies. This improvement at tidal frequencies is due to the relatively large contribution of the tidal currents to the signal at this site, resulting in consistently higher signal-to-noise ratios at these frequencies.

Comparing the measurements by the VMCM and the CMDR in Figure 8, the VMCM is seen to be in good agreement with the CMDR for some of the time, but in disagreement much of the time. It would also appear that the VMCM had an intermittent problem. The VMCM measures the two horizontal components of the current by a pair of orthogonal propellers, so that an intermittent problem with one or both propellers would affect both speed and direction. That there is often a reduction in the speed accompanying large differences in the directions points to a problem with the propellers rather than with the instrument orientation compass.

The histogram of speed for the VMCM (lighter trace) is shown along with that for the CMDR in the lower portion of Figure 9. There is a marked decrease in the number of occurrences of speeds above 20 cm/sec as measured by the VMCM, which again suggests that the unit had some speed sensor problem, particularly at higher speeds. For segments of the data where the VMCM appears to be working properly, agreement between the VMCM and the CMDR is better than that between the Endeco and the CMDR. However, this is not conclusive as we have no means of verifying that the currents were identical at both moorings.

5.2 Strait of Georgia

5.2.1 *Surface mooring GMA.* This site is completely sheltered from the Pacific swell so that the wave conditions are assumed to be due entirely to local winds - the maximum fetch being approximately 60 km. The meteorological data recorded on the surface float are used here as a qualitative indicator of the wave conditions. A Geodyne 850, a Marsh-McBirney 585 and an EG&G VMCM model 630 were suspended close beneath this surface float. The amplitude of the noise was measured using data from the Geodyne burst-sampling current meter. See Section 3.3 and Figure 6 for a description of the moorings.

The time series plots for the first deployment at the central site, GMA, are shown in Figure 11 and 12. The Geodyne recorded four-minute bursts of speed, direction and case orientation with a sample interval of one second. The RMS amplitude of the noise, which we have defined as the

amplitude of the surface-wave-frequency fluctuations in the current as seen by the current meter, was calculated from these bursts of measurements. The average current was calculated for each burst by taking the vector average of 240 one-second samples, then the RMS noise was determined by taking the RMS of the difference between each of these samples and the vector average current. The *noise-to-signal* ratio was taken to be the ratio of this RMS noise to the speed of the current as measured by the Marsh-McBirney 585. The scatter plots and histograms of speed used data filtered by a three-pass moving-average filter of 20 minutes length, then subsampled to 20 minute values. A total of 1024 points was used for these plots and in the power spectra (Figures 13 and 14).

We first examine the lower plots in Figures 11 and 12 which show overlays of the data from the Marsh-McBirney 585 and the Geodyne. The plot labeled "Geodyne-AML vector speed" is the amplitude of the vector average of each burst of current measurements and that labeled "rotor speed" is the average of each of the speeds in the burst. The rotor speed of the Geodyne is much higher than the speed measured by the Marsh McBirney and the differences are significantly correlated with the *noise-to-signal* ratio. The vector speed is in much better agreement with the Marsh-McBirney data, revealing that vector averaging of the burst of samples eliminates a large proportion of the surface-wave-frequency contamination of the measurements. For this to be true, the rotor and vane must be making reasonably accurate measurements of the surface-wave-induced fluctuations, justifying our use of these as a measure of the noise. In the upper left of Figure 13, the scatter plot of vector speed reveals a rather wide spread of points around the line of identical response, even though the histograms of vector speed seem reasonable, excepting speeds less than 15 cm/sec.

Saunders (1980) showed that a VACM Savonius rotor, which is identical to the Geodyne rotor, may give erroneous speeds in the presence of surface-wave-frequency fluctuations in speed. The time constant of these rotors is dependent on the speed of the flow. For the vector average to be accurate, the time constants of the vane and rotor should be small with respect to the period of the fluctuations. Woodward and Appell (1974) indicate that the vane time constant for a VACM is not less than 1.5 seconds and for the Geodyne the figure is similar. Saunders (1980, p759) concludes that the lag in vane response "generally (but not invariably), leads to an overestimate of low-frequency vector-average currents. The overestimate is small (a few percent) in dominant periods of 10 to 15 s and large (circa 25%) when the dominant periods are 3 to 4 s." The

differences in measurements obtained by the Geodyne and the Marsh-McBirney are similar in magnitude to those predicted by Saunders due to vane lag alone at wave periods in the range 3 to 4 seconds. The Geodyne and VACM sensors are almost identical so that Saunders' conclusion should carry directly over to the case of the Geodyne. The wave periods in the three-day time series segments shown in Figures 11 and 12 were in the range 3 to 7 seconds - a little longer than in Saunders' example. It is also possible that the fluctuating vertical component of the current seen by the Geodyne would have contributed significantly to the overestimation of the horizontal component of velocity due to "pumping" of the Savonius rotor.

The power spectra in Figure 14 for the Marsh-McBirney and the Geodyne show reasonable agreement between the two with no definite tendency excepting slightly greater power by the Geodyne at frequencies greater than 0.1 cycles per hour.

The upper part of Figure 11 shows an overplot of the data from the Marsh-McBirney 585 and the VMCM when the tidal currents were large. The agreement in speed is generally very good, with a typical difference of 5 cm/sec. However, at times there are order 10 cm/sec disagreements in the speed, which often correspond with large differences in the direction. This VMCM is the same unit which, in the Queen Charlotte Sound data, showed what was suspected to be an intermittent propeller problem, so we suspect a recurrence. At some time during this deployment, one blade was lost from the upper propeller of the VMCM, although there is no indication in the record to show when this occurred. Also, there can be stratification in this area in calm conditions which may give rise to significant vertical shears. The VMCM propellers, which measure the two components of velocity with respect to the instrument framework, are separated by 40 cm in the vertical so that in the presence of vertical shear there are systematic errors in the measurement of both speed and direction.

In Figure 12 the tidal currents are relatively weak and the winds relatively strong. Consequently the *noise-to-signal* ratio is often greater than 5. Even in these severe conditions, there are long segments of data where the agreement is good and we presume that the VMCM is operating properly at these times. Where the agreement is poor we cannot come to any definite conclusion due to the uncertainty regarding the condition of the VMCM. That the VMCM is malfunctioning at times is clearly seen in the overplot of power spectra in Figure 14. The power seen by the VMCM is much too high at frequencies above 0.1 cph. In spite of this, the scatter plot of speed in the lower left

of Figure 13 confirms that there is considerably better agreement between the VMCM and the Marsh-McBirney than between the Geodyne and the Marsh-McBirney. The relatively long segments of data where the agreement between the VMCM and Marsh-McBirney is excellent leads us to conclude that both of these instruments are capable of good quality current measurements when suspended from a surface float.

5.2.2 *Surface mooring GMB.* The location and mooring configuration for this deployment were identical with that of GMA except for the current meters which consisted of a Neil Brown ACM2, an inverted Marsh-McBirney 585, a Sea Data 620, and a Simrad UCM. With the exception of the Marsh-McBirney 585, which failed during the first day of the deployment due to a defective battery, these instruments all appeared to function normally; a segment of the time series of current vectors is shown in Figure 15.

The data segment for Figure 15 was chosen to show the period of strong winds which occurred on December second and which may be contrasted with the calm conditions immediately preceding. The agreement between these current meters is considerably worse than between those installed on GMA despite similar wind conditions (and presumably sea state). It is unfortunate that the Marsh-McBirney 585 failed, as we feel confident enough of its performance, after comparison with the VMCM, to have used it as a reference for the others. As the absolute performance of these three instruments is unknown for the present mooring configuration (close below a surface float), we have little *a priori* basis for choosing one data set over another to represent the true current.

The Sea Data 620 has an electromagnetic sensor identical with that of the Marsh-McBirney 585 so there is the potential for similar performance. In contrast with the Marsh-McBirney 585, this instrument operates only in burst mode and was set so that each burst consisted of 32 records at 8 second intervals, a total burst length of 256 seconds, all recorded internally. The sensor is sampled at a basic rate of 1 second and internal filtering is done to reduce the 1 second values to 8 second intervals. Each burst was vector-averaged to produce the final data set and this should be equivalent to Marsh-McBirney 585 data, as long as the Sea Data 620 filtering is adequate. With this in mind, we examine the records from the other two instruments relative to those from the Sea Data 620.

In the lower two frames of Figure 15, the speed and direction time-series for the Neil Brown ACM2 and Sea Data 620 are overlaid. It may be seen that during weak winds the

agreement is best and that in moderate to strong winds the agreement is poor, the Neil Brown ACM2 reading much higher than the Sea Data 620. This segment is not typical of the entire time series, which is more closely represented by the data from the first half of December 1st, the winds being light for most of the deployment. The Neil Brown ACM2 often measured speeds considerably less than the Sea Data 620 when the winds were light, but throughout the series showed a strong tendency to overestimate the speed relative to the Sea Data 620 when the wind speed was greater than 5 m/sec .

The speed scatter diagram in the upper left of Figure 16 summarises the disagreement between these instruments with a wide distribution of points about the line of identical response. The tendency to relative overindication of speed by the Neil Brown ACM2 (lighter trace) is also evident in the histograms of speed occurrences in the lower part of the diagram. The data used in the scatter plots, histograms and spectra were reduced to a common fifteen minute sample interval by filtering and subsampling the data from the Sea Data 620 and the Neil Brown ACM2, giving a total of 2048 points for the period shown under "duration" in Table 3.

The power spectra shown in Figure 17 are in remarkable agreement at higher frequencies considering the disparity between the time series data of the Neil Brown ACM2 and the Sea Data 620. At frequencies below 0.02 cph, the higher speeds indicated by the Neil Brown ACM2 during strong winds caused significant increases in power.

The Neil Brown ACM2 had serious problems in this installation, the cause of which is undetermined. Two mechanisms suggest themselves: flow interference and/or air bubbles. The surface float transmits much of the vertical motion of waves to the instrument string along the mooring line. A large vertical velocity past the instrument could place the parcel of water to be measured in the wake of the instrument case or the mirror support structure. It may also be that entrained air bubbles disturb the acoustic measurement process. In later models of the Neil Brown acoustic current meter, introduced soon after this experiment was completed, the problem of wake from the pressure case has been reduced by eliminating the large end cap flange adjacent to the sensors. Whether this modification will significantly improve the performance of the instrument on a surface mooring remains to be determined (see also Spenser and Aubrey, 1986).

The upper part of Figure 15 presents a typical segment of the speed and direction time series for the Simrad UCM and the Sea Data 620. There is reasonable qualitative agreement

between these two instruments during the first of December, but this degraded as the wind speed increased early the next day. The Simrad UCM data shows strong symptoms of aliasing. Unlike the Sea Data, the Simrad UCM does not perform internal averaging to produce samples at rates slower than the fastest sampling rate. This instrument has the capability of burst operation with sample intervals as short as 1.5 seconds, but the sample scheme selected for this experiment for endurance considerations was a burst of six samples at an interval of 8 seconds repeated every 15 minutes. Even with this sparse sampling, the endurance of the instrument was limited to a recording capacity of a little more than 40 days. The inadequacy of the sampling clearly manifests itself in the noise level of the Simrad UCM data, which is strongly correlated with the wind speed. This contamination of the data is certainly due to the aliasing of fluctuations in the current induced by surface gravity waves.

In the lower frame of Figure 16, there is considerable scatter about the line of identical response between the Simrad UCM and the Sea Data 620, though not quite as widely scattered as with the Neil Brown ACM2 - Sea Data 620 pair above. Surprisingly, the histogram of the occurrence of speed shows reasonable agreement in spite of the obvious differences revealed by the time series plots. The overplot of power spectra in the right frame of Figure 17 shows strong disagreement at high frequencies, typical of an aliased signal for the Simrad UCM.

In spite of this aliasing, the agreement between the Simrad UCM and the Sea Data 620 is considerably better than between the Neil Brown and the Sea Data 620, particularly in calmer conditions. The Simrad UCM would seem promising for near-surface applications if *in situ* vector averaging were added or in instances where only short periods of data are required.

5.2.3 *Subsurface mooring GSW.* This mooring was deployed approximately 500 m southwest of the central surface mooring GM, with a cluster of three current meters at the top of the mooring. See Section 3.3, Figure 3, Figure 6 and Plate 1 for details of the location and mooring configuration.

In this instrument cluster were: a Geodyne 850 set to sample at one second intervals for four minutes, repeated every ten minutes; a Dumas Neyrpic CMDR; and an Aanderaa RCM4 with standard Savonius-like rotor. The two latter instruments

employ the same sample scheme - a continuous accumulation of rotor revolutions which is recorded along with a single sample of vane direction once per sample interval (in this case, ten minutes).

All three instruments functioned normally for the entire deployment with the exception of the Digicourse compass in the CMDR which failed after several days. There was also a minor calibration problem with the Geodyne in that there was a misalignment of the vane and compass which caused a direction offset of 40 degrees.

In contrast to the surface moorings where there was considerable wave motion, these instruments had negligible exposure to surface-wave-induced motion. A relatively small signal-to-noise ratio of around 3, computed from the bursts recorded by the Geodyne, was almost perfectly correlated with the speed of the current. Upon closer examination of the bursts of one second samples, we found that the speed was very smooth but that there was considerable high frequency fluctuation in the vane readings with amplitudes of around 15 degrees. The Geodyne has a relatively small vane (cf. Table 1) and we feel that the source of the fluctuations in the vane readings is due to vane motion caused by a combination of mooring motion, vortex shedding from the instrument case, and vane deflection caused by flow around the bars of the cage surrounding the vane. Such motion explains the noise level and the somewhat low speeds computed by vector averaging the bursts of samples measured by the Geodyne. Any errors in direction would have the effect of reducing the vector speed in the true direction by the cosine of the error. The signal-to-noise ratio shown in Figure 18 is thus suspect and should not be used as an indicator of high frequency signal in the current seen by the instruments, except perhaps that due to mooring motion.

In the lower frame of Figure 18 are typical segments of the speed time series from the CMDR and the Aanderaa RCM4. The agreement in speed is almost perfect, except that the CMDR indicates speeds 1-2 cm/sec greater than the Aanderaa throughout the record.

The scatter plot in the lower left of Figure 19 again shows a small, nearly constant offset at higher speeds, but also reveals that the CMDR tended to read slightly lower than the Aanderaa at speeds below 10 cm/sec. The histogram of speed shows this clearly; the darker trace is for the CMDR, which registered much fewer occurrences of speed below 10 cm/sec, except for zero speed.

A tendency to read low at small velocities is characteristic of the CMDR and similar instruments having directional speed sensors which must be oriented into the flow by a vane. At low velocities, depending on the rate of change of direction and upon the stiffness of the swivel arrangement, the sensor may not be well aligned with the flow, causing the speed measurement to be lower than the true speed. In the case of the CMDR, the two bladed propeller stalls when the angle of attack is greater than approximately 40 degrees. This gives rise to the large number of occurrences of zero speed relative to the Aanderaa RCM4.

The Aanderaa RCM4, on the other hand, was fitted with the Savonius-like rotor which has omni-directional response, so the speed is little affected by misalignment with the flow. It should be noted that this is not the case with the new Aanderaa paddle-wheel rotor and that there are problems with this paddle-wheel rotor at low speeds, although not quite as pronounced as with the CMDR (cf. Figure 22).

The upper two frames of Figure 18 show a representative segment of the time series of speed and direction obtained from the Geodyne and the Aanderaa RCM4.

The agreement in speed is good for the most part, with the Geodyne giving speeds consistently lower by a few cm/sec. Occasionally however there are periods where the Geodyne records speeds 5 to 10 cm/sec lower than the Aanderaa, particularly at speeds greater than 20 cm/sec. There is a strong correlation between the difference in speed and the RMS fluctuation within a burst plotted in the lower frame of Figure 18 as discussed previously. The data would be improved somewhat by filtering the direction measurements in some way before taking the vector average of the burst. We have not done so, firstly as we wish to illustrate the behaviour of a small caged vane, and secondly as our first attempts to do so were not very promising due to the multi-valued nature of direction.

If the 40 degree offset due to vane mis-alignment in the Geodyne is ignored the directions indicated by the Geodyne and the Aanderaa RCM4 are in good agreement, typically within 10 degrees. The Geodyne produced a noticeably smoother trace due to the large number of direction samples taken per measurement interval - 240 versus 1 for the Aanderaa RCM4. The upper right frame of Figure 19 does not show as clearly as does the time series the occasional large disagreements between the Geodyne and the Aanderaa RCM4 (Savonius-like), but indicates a nearly constant offset in speed.

Beardsley *et al.* (1981) found similar underestimation of vector speed by the Geodyne 850, again at speeds greater than 20 cm/sec, though our results are not directly comparable as their instrument sampled every 5.27 seconds as opposed to every second in this experiment. They suggest that the cause of this underestimation of speed was the aliasing of surface-wave-induced motion. We obtain a similar result in the absence of such influence and using a faster sample rate. This suggests that the cause of the underestimation is intrinsic to the instrument sensors, although it may be possible to reduce the error by incorporating a low-pass filter for direction into the vector averaging scheme.

The power spectra of the time series of velocity from the Aanderaa RCM4 and the Geodyne are plotted in Figure 20. There is no significant difference between the two except for a slight tendency to higher power by the Geodyne beginning near 1 cph. We take this as further evidence of the high noise level in direction for the Geodyne as discussed above.

To summarise, all three instruments were in good agreement in speed except that the Geodyne tended to underestimate speeds, particularly at speeds greater than 20 cm/sec. At speeds below 10 cm/sec, there was evidence of rotor stalling and mis-alignment of the CMDR with the flow. The directions measured by the Geodyne and the Aanderaa RCM4 were in good agreement. As the compass failed in the CMDR, we must draw on our other experience with this instrument where we found that the direction measurements were similar in quality to the Aanderaa RCM4, the sampling schemes being essentially identical.

5.2.4 *Subsurface Mooring GNE.* This mooring was very similar in configuration to mooring GSW, but with instrument pairs at 50 m and 100 m depths (see Section 3.3, Figure 3 and Figure 6 for details of the mooring location and configuration). The current meters all appeared to function normally for the entire deployment with the exception of the Neil Brown ACM2 which had a defective compass.

At the top of the mooring was a Geodyne 850 and an inverted Neil Brown ACM2. In the upper frame of Figure 21 the speed time series from this pair of instruments are overplotted and it may be seen that the Geodyne is consistently underestimating speed relative to the Neil Brown ACM2. This disagreement in speed is very similar to that found between the Geodyne and the Aanderaa RCM4 on mooring GSW, but with slightly greater offset and more scatter (cf. the lower left of Figure 22).

One would expect the Neil Brown ACM2 to produce a high quality measurement in this rather quiet application, so we have used the Neil Brown ACM2 as a reference. The agreement between the Geodyne and the Neil Brown ACM2 is noticeably worse than between the Geodyne and the Aanderaa RCM4, with the former pair having more scatter, an offset of 3 cm/sec and a slight difference in sensitivity. That there is better agreement between the Geodyne and the Aanderaa RCM4 may well be due to very similar - but not necessarily accurate - response to speed of their respective Savonius and Savonius-like rotors.

At 100 m depth were two Aanderaa RCM4's, one with the well established Savonius-like rotor and the other fitted with the paddle-wheel rotor. The agreement between these two instruments was excellent; indeed we had to apply offsets in the lower two frames of Figure 21 to separate the traces. The time series plots of direction in the middle frame of Figure 21 are virtually identical with only occasional small phase shifts. There is more variation in the speeds than there is in direction but for the most part the differences are less than 2 cm/sec and appear to be random except at speeds below 5 cm/sec. It was evident from examination of the time series plots that the paddle-wheel rotor consistently underestimated very low speeds relative to the Savonius-like rotor.

The scatter plots and histograms of speed in the upper frames of Figure 22 confirm the relative response seen in the time series plots and also reveal a systematic non-linearity in relative speed. The scatter plot covering the full range of speed indicates, relative to the Savonius-like rotor, that the paddle-wheel rotor has slightly higher response to speed in the range 10 to 20 cm/sec and slightly lower response at speeds greater than 20 cm/sec. At very low speeds - below 5 cm/sec - the tendency of the paddle-wheel current meter is clearly to lower sensitivity (see the right hand frame of Figure 22). Tow tank tests by Aanderaa Instruments have shown that the paddle-wheel rotor does not have a significantly higher threshold than does the Savonius-like rotor (D. Renfroe, personal communication). Rather, it is the uni-directional nature of the paddle-wheel rotor with its semi-circular shield which we feel gives rise to the low response through misalignment with the flow. This low speed performance problem is very similar to that of the CMDR on mooring GSW - the vane may not orient the speed sensor into the flow when a direction change occurs with speed less than approximately 5 cm/sec.

For each of the Aanderaa RCM4's, the power spectra were virtually identical and are not shown; also not plotted are

power spectra for the pair of current meters at 50 m due to the failure of the compass in the Neil Brown ACM2.

As might be expected where there is no influence from surface-wave-induced motion, the performance of the current meters on mooring GNE was good to excellent, mostly within a few cm/sec. The Geodyne gave a consistent underestimation of speed relative to the Neil Brown ACM2, similar to that seen on mooring GSW, but we can make no statement regarding the directions due to the failure of the compass in the Neil Brown ACM2. The pair of Aanderaa RCM4's were in remarkably good agreement with some relative non-linearity and low speed stalling evident with the paddle-wheel rotor.

5.3 Hecate Strait

As indicated in Figures 1 and 4, this site has moderate exposure to surface waves with a 300 km fetch to the southeast, but is mostly protected from longer period Pacific Ocean swell. The objective of this study was to evaluate the performance of the Marsh-McBirney 585 on a surface mooring relative to measurements from a sub-surface mooring and to investigate the performance of the Aanderaa RCM4 on a shallow sub-surface mooring. For details of the configuration of the moorings see Section 3.4 and Figure 7.

The surface-wave field in this experiment was inferred from a combination of bottom-pressure records and wind speed. Bottom pressure was recorded in bursts of one-second samples every two hours, but the attenuation of the surface-wave-induced pressure fluctuation limited the detection of surface waves to periods longer than 5 seconds. The anemometer data can be used to estimate energy levels in the higher frequency portion of the wave spectrum.

Each burst of bottom pressure data consisted of a time series of 128 samples. For each of these bursts, a single predominant frequency was taken to approximate the low frequency portion of the the wave field, accounting for most of the energy in the range of period 5 to 20 seconds. For these periods, the magnitude of the wave-induced fluctuation in the current was computed by numerically solving the surface gravity wave equation for intermediate depth. This is labelled "Computed wave-induced current" in the lower frames of Figure 23 and Figure 24 and was computed for the instrument cluster on the subsurface mooring.

For the period July 6-8, the low frequency portion of the wave field was relatively weak, with periods in the range 15 to 17 seconds and amplitudes at the surface of 10-30 cm. Shortly after mid-day on July 8 the wind speed began to

rise, reaching a maximum speed of approximately 12 m/sec early on July 9. A correspondingly rapid increase in the low frequency wave field occurred early on July 9 with a new dominant period of 7 seconds. This increase in wave energy resulted in a marked increase in the wave-induced motion of both the surface and subsurface moorings. The wave-induced motion of the surface mooring is much more severe than that of the subsurface mooring as the full force of the waves operates directly on the surface float.

5.3.1 *Marsh-McBirney 585* The segment of the time series shown in Figure 23 was chosen for the period of strong winds on July 9, which may be contrasted with the preceding period of relatively calm conditions. The wind 3.5 m above the surface is shown in the upper frame of Figure 23 and Figure 24 and the magnitude of the computed wave-induced fluctuation in the current, as discussed above, is shown in the lower frames along with the RMS fluctuation in bottom pressure.

The currents measured by the two Marsh-McBirney 585s, one on the surface mooring and the other on the subsurface mooring, are shown in Figure 23. The agreement between the two is good, considering that the instruments were separated by 500 m in the horizontal and in the vertical by as much as 10 m depending on the stage of the tide. There is no obvious change in the character of the measurements from the surface mooring with changes in sea state and the agreement is typically within 10 cm/sec and 20 degrees. The scatter plot of speed in the lower right of Figure 25 summarises the speed comparison over the period shown under duration in Table 3 with a nominal 10 cm/sec spread about the line of identical response.

The power spectra shown in Figure 26 are in reasonable agreement, but away from the main tidal frequencies there is a tendency towards higher power of the measurements from the surface mooring. It is tempting to conclude that this is due to the aliasing of surface-wave-induced motion, but the differences are not large enough to be conclusive without some independent means of verifying that the currents were identical at each site.

In spite of the inherent limitations of this experiment, the agreement between the measurements from the surface mooring and those from the subsurface mooring provides confirmation of our earlier conclusion that the Marsh-McBirney 585 is capable of good quality measurements on a surface mooring.

5.3.2 *Aanderaa RCM4 with Savonius-like rotor* The time series segment in Figure 24 is for the same period as for Figure 23 with a plot of current speed and direction from the three subsurface current meters. The data from the two Aanderaa RCM4's was evaluated using the data from the Marsh-McBirney 585 as reference.

An examination of the time series reveals that the Aanderaa RCM4 with the Savonius-like rotor consistently gives a speed greater than that measured by the Marsh-McBirney 585, particularly when the wave-induced fluctuations in speed are similar to or greater than the average speed. This response is not unexpected due to the omnidirectional response to velocity of the Savonius-like rotor and, in all fairness, this is likely a far more severe operating environment than was ever envisaged by the original designers. However, these instruments have been used in large experiments in very similar conditions - one example is the study of low frequency currents in the Gulf of Alaska as described by Pearson *et al.* (1981). They concluded that satisfactory results for seasonally-averaged currents can be obtained using Aanderaa RCM4 current meters with the subsurface float as shallow as 18 m in spite of significant wave-induced fluctuations at this depth.

The upper right of Figure 25 presents a scatter plot and histogram of speed for the Aanderaa RCM4 (with Savonius-like rotor) versus the Marsh-McBirney 585. The plots are based on 21 days of unfiltered data at the original 15 minute sample interval, as shown under duration in Table 3. The wave conditions during this period were mostly quite weak with peak wave-induced velocities of approximately 10 cm/sec. Even in these quiet conditions, there are many points far removed from the line of identical response, confirming the strong tendency of the Aanderaa RCM4 with Savonius-like rotor to bias toward higher speed in the presence of relatively weak wave-induced fluctuations in the current. Examining the histograms of speed, there are very few occurrences below 10 cm/sec by the Aanderaa RCM4 - the lighter trace - presumably due to erroneous response to wave-induced motion. There are more than twice as many occurrences of speed between 10 cm/sec and 20 cm/sec by the Aanderaa RCM4 relative to the Marsh-McBirney 585. At speeds greater than 25 cm/sec, the Aanderaa RCM4 indicated many more occurrences of a particular speed relative to the Marsh-McBirney 585, with the histograms gradually converging with increasing speed as the signal-to-noise ratio improves.

It is clear that, in this experiment, the Aanderaa RCM4 with Savonius-like rotor gave results which were strongly biased toward high speed. A number of mechanisms for this are

discussed in Woodward (1985) and Hammond *et al.* (1986), all of which are in some way related to wave-induced motion.

It is often difficult to assess the effect of speed errors on long term means due to the modulation of speed by the direction. For example, a constant speed offset of any amplitude would have no effect on the mean if the flow was one-dimensional, bi-directional, and if the total time was equally distributed between the two directional modes. Conversely, the long term mean of a mainly uni-directional flow would be strongly affected by a speed offset, for there would be little cancellation in the averaging.

In this experiment there are large and variable speed errors, but the flow is mainly bi-directional so that much of this speed error cancels in the mean. For the Marsh-McBirney 585 we obtain a mean speed of 28.7 cm/sec compared with 35.9 cm/sec for the Aanderaa RCM4 with Savonius-like rotor (cf. Table 3). The corresponding amplitudes of the M2 tidal constituent are 37.7 cm/sec and 42.5 cm/sec. Relative to the Marsh-McBirney 585, the Aanderaa RCM4 measures 25% high in the mean and 13% high in the M2 tidal amplitude. If the flow were biased toward one direction, one would expect the errors in the mean to rise dramatically.

The power spectra of the data from the Aanderaa RCM4 with Savonius-like rotor and the Marsh-McBirney 585 are plotted in the left of Figure 27. The Aanderaa RCM4 results in significantly greater power at all frequencies except at the diurnal and semi-diurnal tidal periods. The spectra are remarkably similar to those of Pearson *et al.* (1981) from the Gulf of Alaska which also have a large proportion of the energy at tidal frequencies. With most of the higher speeds generated by tidal forcing, and keeping in mind that the errors in speed are much less at higher speeds, we conclude that the tidal signal is measured with substantially greater accuracy than either the higher or lower frequency signals. The anomalous agreement in the spectral power between the Aanderaa RCM4 with Savonius-like rotor and the Marsh-McBirney 585 at tidal frequencies can be explained by this speed dependence of the error.

In contrast to our results, Halpern and Pillsbury (1976) found that current meters using Savonius rotors gave a uniform increase in power at frequencies less than 0.7 cph when subject to increased wave motion. This result is crucial to the argument of Pearson *et al.* (1981, p 1225) that "Since rotor pumping tends to raise tidal and lower frequency bands by an approximately constant proportion, a comparison of winter and summer tidal amplitudes will indicate contamination of the current records at tidal and

lower frequencies." The results of our experiment in Hecate Strait, where the operating conditions were similar to those in the Gulf of Alaska, clearly demonstrate that the tidal signal is a poor indicator of current meter performance in these conditions and extrapolation to other frequency bands may be misleading.

In pursuit of a more reliable means of predicting the performance of the Aanderaa RCM4, Hammond *et al.* (1986) made a series of experiments in a flume to simulate wave-induced motion superimposed on a mean flow. In contrast to their experiments, we had no control over the wave environment and had indirect wave measurements only for the range of periods 5 to 20 seconds. We attempted to correlate the errors with wave amplitude, period and mean current speed, but the scatter was quite overwhelming, so we will only make a general statement concerning the most predominant modes.

There were many measurements when mean speeds in the range 5 to 10 cm/sec were accompanied by peak wave-induced velocity around 10 cm/sec and in this mode errors were large - often 50% to 200% - compared with errors in the vicinity of 100% predicted by Hammond *et al.* (1986) in similar conditions. At mean speeds greater than 20 cm/sec, the errors are smaller - typically 30% high. These variations of the errors with peak wave orbital velocity and mean speed are in good general agreement with the results of Hammond *et al.* (1986), indicating that the errors found in the flume experiments are representative of actual operational errors for an Aanderaa RCM4 equipped with a Savonius-like rotor.

At peak wave orbital speeds near 40 cm/sec, which are outside the range considered by Hammond *et al.*, the errors at low mean speed were much greater - 200% to 500% - and as the mean speed approached the peak wave orbital speed, the errors were commonly around 50%. At higher mean speeds, the errors were somewhat less, keeping in mind that there was much variation in the error for what would seem to be similar operating conditions.

In summary, the speed error of the Aanderaa RCM4 with Savonius-like rotor is not a simple function of signal-to-noise ratio as one might expect for an omni-directional sensor. Rather, the errors are very large at low speeds when the wave-induced fluctuations in velocity are comparable to or greater than the mean current, and diminish as the mean speed increases.

5.3.3 *Aanderaa RCM4 with paddle-wheel rotor* Returning to the time series plots in Figure 24, it may be seen that the Aanderaa RCM4 with paddle-wheel rotor is in good agreement

with the Marsh-McBirney 585 even during times of strong wave-induced motion. The speeds typically agree within 5 cm/sec, usually biased toward lower speed, but the directions are noisy, particularly at low speeds. The cause of this speed bias is thought to be due to misalignment of the speed sensor with the flow in the presence of wave motion (cf. Woodward, 1985). As the wave motion becomes more intense, the tendency at low speed is to overestimate speed (see the period of speeds around 10 cm/sec on July 9). The increased wave motion presumably generates spurious rotor motion which counters the bias toward lower speed caused by misalignment of the unidirectional speed sensor with small wave-induced fluctuations in flow.

The scatter plot in the lower left of Figure 24 summarizes the response over the period shown under duration in Table 3, with a general tendency for the Aanderaa RCM4 with paddle-wheel rotor to be biased toward lower speed. Note that this appears as a shift in speed rather than as gain error and that the scatter decreases as speed increases, indicating that the effect is due to wave action. This is confirmed by the histograms of the occurrence of speed - the darker trace is for the Aanderaa RCM4.

This bias toward low speed is contrary to the results of the flume experiments by Hammond *et al.* (1986) which indicate overestimation of speed in the presence of surface-wave-frequency fluctuations. In these flume experiments, the sensor assembly was mounted on an oscillating carriage so that only one horizontal component of fluctuation in the flow could be simulated. As installed on a mooring, the instrument may be subjected to a fluctuation in speed in any component and is free to rotate in response. This freedom allows a variation in the angle of attack of the speed sensor for the moored instrument which was fixed in the flume experiments. That the flume experiments do not reproduce the bias toward low speed seen in our intercomparison is presumably due to misalignment of the speed sensor of the moored instrument with wave-induced motion.

The spectra in the right of Figure 27 for the Aanderaa RCM4 with paddle-wheel rotor and the Marsh-McBirney 585 are almost identical, except for a slight tendency of the Aanderaa RCM4 for higher power at frequencies above 0.1 cph. This is likely due, for the most part, to the aliasing of direction.

In the presence of wave motion, the Aanderaa RCM4 with paddle-wheel rotor is certainly a vast improvement over the Aanderaa RCM4 with Savonius-like rotor, but this is more a

measure of the poor performance of the Savonius-like rotor in these conditions than anything else. In the mean, speeds were 8% low relative to the Marsh-McBirney 585 (cf. Table 3). The inherent limitations of the large vane and the severe aliasing of direction have not been addressed in this instrument. The wave exposure in this study is likely near the upper limit for this instrument, which certainly could not tolerate the intensive motion of a surface mooring in any but the calmest of conditions.

6. SUMMARY OF CURRENT METER PERFORMANCE

In an intercomparison experiment such as this, evaluation of the performance of any particular instrument can, in the strictest sense, be only relative. In several cases however, our confidence in the data from another current meter in the cluster allows us to imply a more absolute measure of performance. The following summaries tend to be qualitative as there is a wide range of operating conditions involved and the reader is referred to the discussion in Section 5 for further detail. Table 3 may be used as a cross-reference between instrument types and the various moorings on which these were deployed.

6.1 Aanderaa RCM4 with Savonius-like rotor

In a steady flow (or on a subsurface mooring below wave action), the Aanderaa RCM4 with Savonius-like rotor agreed very well with other instruments of similar sampling scheme, but in the presence of a fluctuating flow, particularly where there was significant surface-wave-induced motion, errors were often large and comparable in magnitude to that of the average wave-induced component of velocity. The flume experiments of Hammond *et al.* (1986) provide estimates of these errors which are consistent with those found in our experiments. We confirm the conclusion of Saunders (1976, p. 255) that the Aanderaa RCM4 with Savonius-like rotor "should not be used where surface wave frequency fluctuations are even a small fraction of the signal."

6.2 Aanderaa RCM4 with paddle-wheel rotor

In the absence of high frequency fluctuations in the flow, the Aanderaa RCM4 with paddle-wheel rotor was very similar in performance to the Aanderaa RCM4 with the Savonius-like rotor except that the response to speed was slightly non-linear with reduced sensitivity at speeds below 5 cm/sec.

In the wave zone, the paddle-wheel rotor and semi-circular shield was a significant improvement over the omni-

directional Savonius-like rotor, but there was a tendency for bias toward low speeds. This bias is presumably caused by misalignment of the speed sensor with the instantaneous velocity, resulting in reduced sensitivity to speed. There was serious aliasing of direction in the presence of high frequency fluctuations in the flow, as with the earlier Aanderaa RCM4.

6.3 Dumas Neyrpic model CMDR modified by Applied Microsystems Ltd.

On a shallow sub-surface mooring where there was moderate wave motion, this current meter agreed reasonably well with others nearby, but the degree of contamination by wave-induced motion could not be determined. When moored at 50 m, the Dumas Neyrpic CMDR performed very well, but with a tendency to read high by a few cm/sec except at speeds below 5 cm/sec where there is some loss of sensitivity which we attribute to misalignment with the flow. This is a very respectable performance for an instrument originally designed in the 1950's.

6.4 EG&G VMCM model 630

The VMCM was evaluated on surface moorings only. The amplitude of surface-wave-induced fluctuations in the mean flow is much greater in applications using a surface float relative to what would be found in the case of a shallow sub-surface mooring.

The particular instrument which was used in our experiments had intermittent problems, but there were relatively long periods when it seemed to be operating correctly. During these periods the agreement with the Marsh-McBirney 585 was very good, indicating that this instrument is capable of high quality measurements when moored with a surface float. The rotors are susceptible to entanglement in weed and the like although there is some protection afforded by the surrounding cage.

6.5 Endeco type 174

The Endeco type 174 current meter was tethered to a light surface mooring which was in turn tethered to the top of a subsurface float at 7 m depth.

The speeds measured by the Endeco were consistently higher than those obtained from the subsurface mooring, presumably due to spurious rotor revolutions induced by wave action. The direction measurements were noisy as one might expect from an current meter without vector averaging capability.

However, considering the simplicity and low cost of this instrument, the performance was surprisingly good.

6.6 Geodyne 850 modified by Applied Microsystems Ltd.

The Geodyne 850 current meter was a predecessor to the EG&G VACM with a very similar sensor configuration. The instruments used in this experiment were modified by Applied Microsystems Ltd. to record in bursts with a sample rate within each burst of one second.

On subsurface moorings, mounted close beneath the uppermost float at 50 m, the Geodyne consistently recorded lower speeds than other instruments in the clusters. This is consistent with the findings of Beardsley *et al.* (1981). The underestimation of speed by this instrument is attributed to high frequency fluctuations in the vane direction which gives rise to errors in the instantaneous velocity components comprising each burst and so to the vector average velocity.

Moored at 6 m beneath a surface float, the Geodyne gave average rotor speeds much in excess of the average speed, characteristic of an omni-directional speed sensor in the presence of wave motion. The vector average speed calculated for each burst was in qualitative agreement with the speed measured by other instruments in the cluster, but generally tended to overestimate the speed and was inconsistent in its response.

6.7 Marsh-McBirney 585

Our test deployments of the Marsh-McBirney 585 concentrated on near-surface applications with the instrument suspended beneath a surface float at a nominal depth of 5 m. For this configuration, we found that wave orbital velocities in the vicinity of 50 cm/sec were not uncommon.

The Marsh-McBirney was in very good agreement with other instruments in the cluster or with an identical instrument on a nearby shallow subsurface mooring. This demonstrates quite conclusively that the Marsh-McBirney 585 is capable of high quality measurements when moored from a surface float. Unfortunately the instruments were not without reliability problems, not with the sensor, but with the digital electronics and recorder.

6.8 Neil Brown ACM2

At 50 m on a subsurface mooring, the Neil Brown ACM2 produced an excellent record of speed but the failure of the compass prevented a more complete evaluation.

Mounted 6 m below a surface float, the Neil Brown instrument showed serious problems. There was a strong tendency for overestimation of speed, particularly in the presence of more intense wave motion, but the response was inconsistent.

6.9 Sea Data 620

The Sea Data 620 employs a Marsh-McBirney sensor identical with that fitted to the Marsh-McBirney 585 and so is potentially capable of similar performance. However, the poor quality of the data obtained from the other instruments in the cluster of the test deployment of the Sea Data 620 leaves us with an inconclusive result.

6.10 Simrad UCM model 37

The data from the Simrad UCM model 37 showed strong aliasing of surface-wave-induced motion. This was due to an inadequate sample rate which was forced by the duration of the experiment.

The data indicated that the instrument may well be capable of good quality measurements if the storage capacity were improved or on-board vector averaging incorporated.

7. CONCLUSIONS

It has been widely recognised for more than a decade that the effects of surface-wave-induced motion are the dominant source of errors in the measurement of velocity by current meters moored near the surface. We found that for one of our surface moorings, the ratio of the surface-wave-induced fluctuations in velocity to the average current velocity was commonly in the range two to five. In these severe operating conditions there were large differences in current meter performance.

Only the EG&G VMCM model 630 and the Marsh-McBirney 585 appeared to be capable of producing quantitative velocity measurements on a surface mooring in the presence of a moderate wave field. Our testing of the Sea Data 620 was inconclusive. The other current meters moored near the surface showed large differences in performance due to limitations in the individual sensor designs and/or the

sampling techniques. On a subsurface mooring with the floatation as shallow as 10 m below the surface, the Aanderaa RCM4 with paddle-wheel rotor gave reasonable speeds, but the direction was severely aliased. Those current meters moored at sufficient depth to be free of the influence of surface waves were in good agreement - typically within 2 cm/sec and 5 degrees. Small systematic errors were evident, reflecting the different measurement techniques employed on the various instruments.

Our analysis indicates that it was important to examine the data from many points of view and that there was no particular analysis technique which provided the most insight; spectral analysis was among the least definitive means of determining current meter performance.

8. ACKNOWLEDGEMENTS

A number of current meter manufacturers generously loaned instruments for this intercomparison. It is a tribute to their confidence in their product that they did so in the face of Murphy's universal law of current measurement. The Aanderaa RCM4 with paddle-wheel rotor was provided by Aanderaa Instruments, Victoria, B.C. EG&G provided the VMCM model 630 and Rick Comoglio of EG&G assisted in its set-up for the first deployment. Endeco provided the Endeco type 174 including translation of the data. Richard Espy of Marsh-McBirney assisted in the set-up of the Marsh-McBirney 585 for its first deployment. Sea Data provided the Sea Data 620 and 635-12 as well as the services of Winfield Hill who prepared them for deployment. Simrad Houston provided the Simrad UCM model 37 and transcription of the data tape.

The technical assistance was provided by Fred Hermiston, John Love and Bruce Canning as well numerous other IOS staff. Arctic Sciences Ltd. prepared the Neil Brown ACM2's for deployment. John Peart of Interact unraveled the mysteries of the many different data formats in this project and Anne Cave produced the computer graphics. The drafting of the figures was done by Mike Cannon. We also acknowledge the assistance of Jim Bull of CCIW in translating the Sea Data format tapes. Bill Crawford provided valuable comments on the manuscript. We gratefully acknowledge the contribution of the officers and crew of the vessels CSS *Parizeau* and CSS *Vector* in successfully deploying and recovering the moorings for this experiment. All field work and analyses were funded by the Department of Fisheries and Oceans.

9. REFERENCES

Beardsley, R.C., W.C. Boicourt, L.C. Huff, J.R. McCullough and J.Scott (1981) CMICE: A near-surface current meter intercomparison experiment. *Deep-Sea Research*, **28A**, 1577-1603.

Boicourt, W.C. (1982) The recent history of current measurement: an underview. Proceedings of the IEEE second working conference on current measurement. Hilton Head, South Carolina, 9-18.

Gartner, J.W. and R.C. Oltmann (1985) Comparison of recording current meters used for measuring velocities in shallow waters of San Francisco Bay, California. *Oceans '85 Conference Record, Volume 2*, **E7**, 731-737.

Halpern, D. (1980) Moored current measurements in the upper ocean. In: *Air-Sea Interaction*. F. Dobson, L. Hasse and R. Davis, Ed. Plenum Publishing Corp., New York, N.Y. p. 127-140.

Halpern, D., R.D. Pillsbury and R.L. Smith (1974) An intercomparison of three current meters operated in shallow water. *Deep-Sea Research*, **21**, 489-497.

Halpern, D. and R.D. Pillsbury (1979) Influence of surface waves on sub-surface current measurements in shallow water. *Limnology and Oceanography*, **21**, 611-616.

Hammond, T.M., C.B. Pattiaratchi, M.J. Osborne and M. Collins (1986) Field and flume comparisons of the modified and standard (Savonius-rotor) Aanderaa self-recording current meters. *Deutsche Hydrographische Zeitschrift* **39**, 41-63.

Kuhn, H., D. Quadfasel, F. Schott and W. Zenk (1980) On simultaneous measurements with rotor, wing and acoustic current meters, moored in shallow water. *Deutsche Hydrographische Zeitschrift* **33**, 1-17.

Pashinski, D.J. (1985) Comparison of current meters in a tidally dominated flow. *Oceans '85 Conference Record, Volume 2*, **E7**, 738-741.

Pearson, C.A., J.D. Schumacher and R.D. Muench (1981) Effects of wave-induced mooring noise on tidal and low-frequency current observations. *Deep-Sea Research*, **28A**, 1223-1229.

Saunders, P.M. (1976) Near-surface current measurements. *Deep-Sea Research*, **23**, 249-257.

Saunders, P.M. (1980) Overspeeding of a Savonius rotor. *Deep-Sea Research*, **27A**, 755-759.

Spenser, W.D. and D.G. Aubrey (1986) Field performance of NBIS Smart ACM's with EG&G Sea Link VMCM's. *Oceans '86 Conference Record, Volume 2*, 406-409.

Unesco (1970) An intercomparison of some current meters. *Unesco technical papers in marine science*, **11**, 70pp.

Weller, R.A. and R.E. Davis (1980) A vector measuring current meter. *Deep-Sea Research*, **27A**, 565-581.

Woodward, M.J. (1985) An evaluation of the Aanderaa RCM4 current meter in the wave zone. *Oceans '85 Conference Record, Volume 2*, **E8**, 755-762.

Woodward, W.E. and G.F. Appell (1973) Report on the evaluation of a vector averaging current meter. *NOAA-TM-NOS-NOIG-1*.

TABLES

INTENTIONALLY BLANK

TABLE 1. Characteristics of current meters with mechanical speed sensors.

	Aanderaa RCM4 Savonius-like	Aanderaa RCM4 Shrouded Paddle	AML modified Geodyne 850	AML modified Neyrpic CMDR	Endeco Type 174	EG&G VMCM MODEL 630
Speed Sensor						
Type	6-cup rotor Savonius-like carbide pin bearings	6-bladed shrouded paddle wheel carbide pin bearings	4-cup Savonius rotor, carbide pin bearings	2-bladed propellor stainless steel ball bearings in oil bath	8-bladed propellor glass ball bearings in delrin races	pair 5-bladed propellors each axis, stainless steel ball bearings
Diameter (cm)	10.5	10	16	10	37	22
Height (cm)	7	5	17			
Axis	Vertical	Vertical	Vertical	Horizontal	Horizontal	Horizontal
Range (cm s^{-1})	2.5 to 250	3-175*		1 to 500	0-670	
Threshold (cm s^{-1})	2.0	3	1.8	1	2.6	0.9
Resolution (cm s^{-1})	0.3	0.3	2.2	0.5	2.6	0.15
Sampling mode	Continuous	Continuous	Burst (60-660)	Continuous	Continuous	Vector average
Sampling interval	Once per record	Once per record	1 s	Once per record	Once per record	0.25-2.0 s
Direction Sensor						
Type	Vane rotating entire instrument about spindle	Vane rotating entire instrument about spindle	Caged vane carbide pin bearings on instrument axis	Vane 1.6 m from axis of rotation on in-line swivels	Impeller duct serves as vane	Vector average of orthogonal rotors
Vane size (cm)	37 x 100	37 x 100	9.1 x 17.2	20 x 20	40 diameter	none
Compass						
Type	Clamped potentio-meter	Clamped potentio-meter	Optical disc	Optical disc	Optical disc	Flux gate
Resolution	0.35°	0.35°	1.4°	1.4°	1.4°	1.4°
Sampling Interval	Once per record	Once per record	1 s	Once per record	Once per record	0.25 - 2.0 s
Physical						
Length (m)	1.4	1.4	1.8	2.2	0.9	2.1
Weight in Air (kg)	26.6	26.6	60	75	14	55
Weight in Water (kg)	17.3	17.3	25	20	0	29
Type of Attachment	In-line spindle	In-line spindle	In-line, sensors in integral cages	In-line with separate swivels	Rope tether and clamp	In-line, caged

TABLE 2. Characteristics of current meters with electromagnetic or acoustic speed sensors.

	Marsh McBirney 585	Neil Brown ACM2	Sea Data 620	Sea Data 635-12	Simrad UCM
Speed Sensor					
Type	3" spherical electro-magnetic two pair protruding electrodes	2-axis acoustic	3" spherical electro-magnetic two pair protruding electrodes	3" spherical electro-magnetic two protruding electrodes	3-axis acoustic
Range (cm s^{-1})	0-300	0-300	0-300	0-300	0-250
Resolution (cm s^{-1})	0.15		0.2	0.2	0.2
Sampling mode	Vector average of burst	Vector average	Burst (8-128)	Burst (64-2048)	Burst (1-8192)
Sampling interval	1 s	Continuous	4-64 s	0.5-4 s	1.5-32 s
Direction					
Type	Vector average of u + v components	Continuous vector average of u + v components	Burst sample of x,y components and compass	Burst sample of x,y components and pressure	Burst sample of u,v,z, components and compass
Compass					
Type	Optical disc	Flux gate	Optical disc	Optical disc	Clamped potentiometer
Resolution	1.4°		1.4°	1.4°	3°
Sample Interval	1 s	Continuous	4-64 s	Once per burst	1.5-32 s
Physical					
Length (m)	1.5	1.2	1.5	1.5	0.9 m
Weight in Air (kg)	43	34	40	36	
Weight in Water (kg)	18	13	15	14	27
Type of Attachment	In-line	In-line	In-line	In-line	In-line in separate load cage

TABLE 3. Current meter deployment details.

Current Meter (type, mooring, depth)		Duration	Sample Mode	Sample Interval (min.)	Filter Length (min.)	Mean Speed (mm/s)	Resultant Vector Speed	Resultant Vector Direction	Mean u (mm/s)	Mean v (mm/s)
VHDH	G5S, 5 m	May 30 - June 20	Vector Average	15	60	149	Direction problems			
Endeco	G5A, 5 m	May 30 - June 20	Continuous	4	60	197	31	160	-29	11
AML-Geodyne	G5A, 6 m	No data	Burst	15	Hardware faults - digital section					
AML-CMDR	G5A, 7 m	May 30 - June 20	Continuous	15	60	151	15	169	-15	3
AML-Geodyne	GMA, 6 m	October 15-29	Burst	5	20	172	63	Vane alignment error		
Marsh McBirney	GMA, 8 m	October 15-29	Burst	5	20	175	81	157	-75	32
VHDH	GMA, 9 m	October 15-29	Vector Average	4	20	173	94	173	-93	11
Neil Brown	GMB, 6 m	November 4-25	Vector Average	1	15	204	23	123	-13	19
Marsh McBirney	GMB, 6 m	No data	Burst	5	Hardware fault - digital section					
Sea Data 620	GMB, 8 m	November 4-25	Burst	7.5	15	179	46	106	-13	44
Simrad	GMB, 10 m	November 4-25	Burst	15	15	176	28	146	-23	15
AML-Geodyne	GSW, 50 m	November 4-18	Burst	10	Unfiltered	128	78	Vane alignment error		
AML-CMDR	GSW, 50 m	November 4-18	Continuous	10	Unfiltered	150	Defective compass			
Aanderaa RCM4	GSW, 50 m	November 4-18	Continuous	10	Unfiltered	140	88	62	41	77
AML-Geodyne	GNE, 50 m	November 4-18	Burst	5	10	126	80	Vane alignment error		
Neil Brown	GNE, 50 m	November 4-18	Vector Average	1	10	159	Direction defective			
Aanderaa-Paddle	GNE,100 m	November 4-18	Continuous	5	10	150	111	68.8	39.9	103.1
Aanderaa RCM4	GNE,100 m	November 4-18	Continuous	5	10	149	110	68.3	40.4	101.8
Sea Data 635-12	GTR, 39 m	Not analyzed	Burst	4 hr.	Only five days record - bottom mounted					
Marsh McBirney	WSS, 5 m	June 15 - July 27	Burst	15	Unfiltered	278	51	318	38	-34
Marsh McBirney	WOS, 12 m	June 15 - July 27	Burst	15	Unfiltered	287	37	8	37	5
Aanderaa-Paddle	WOS, 12 m	June 15 - July 27	Continuous	15	Unfiltered	264	29	355	29	-2
Aanderaa RCM4	WOS, 13 m	June 15 - July 27	Continuous	15	Unfiltered	359	38	17	37	12

INTENTIONALLY BLANK

FIGURES

INTENTIONALLY BLANK

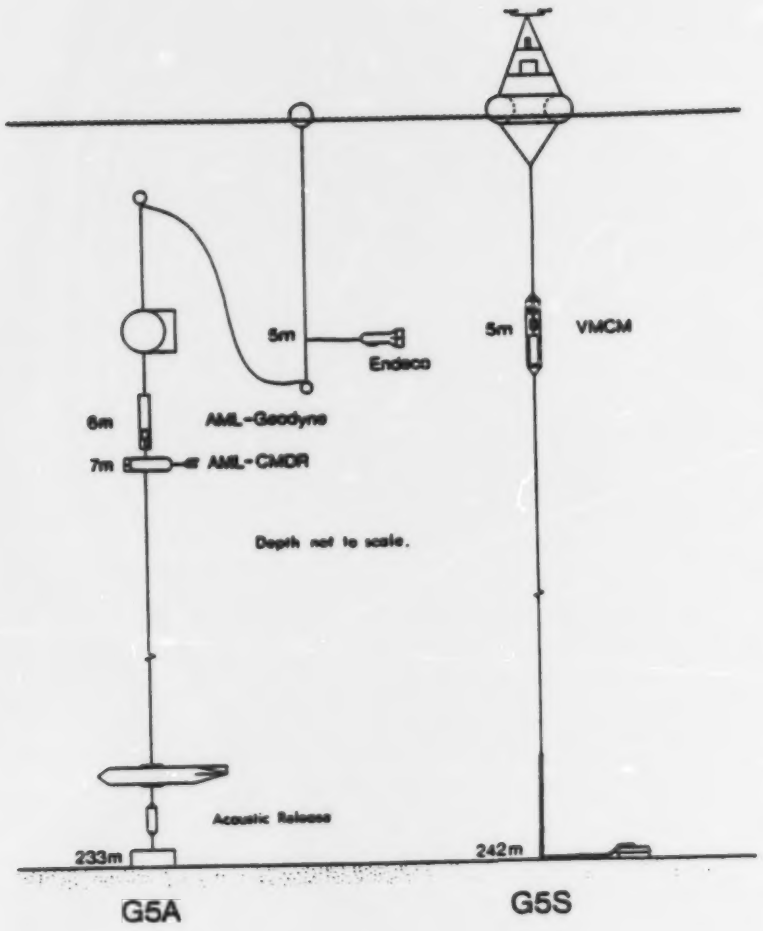

Figure 5. Moorings in Queen Charlotte Sound.

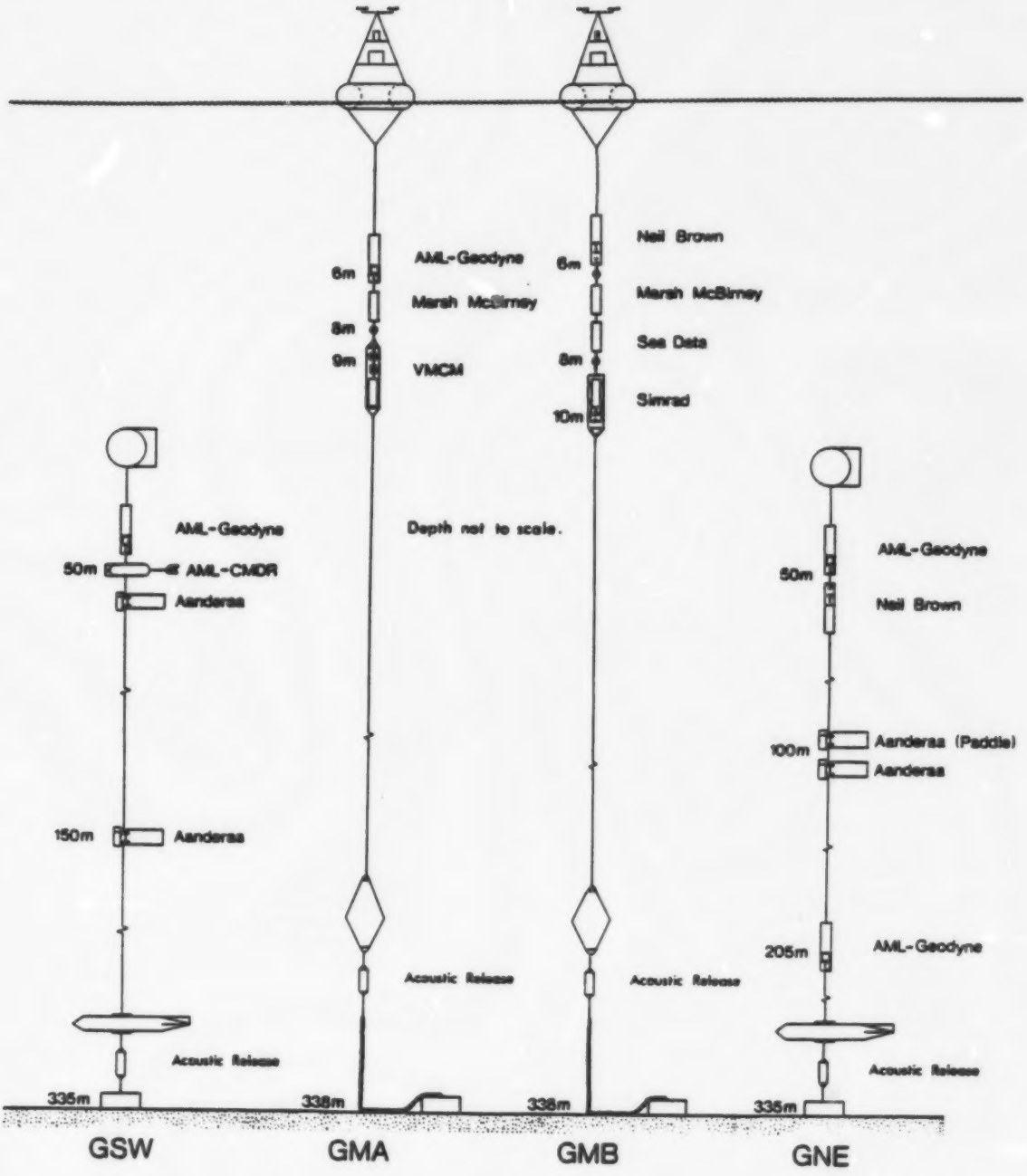

Figure 6. Moorings in the Strait of Georgia.

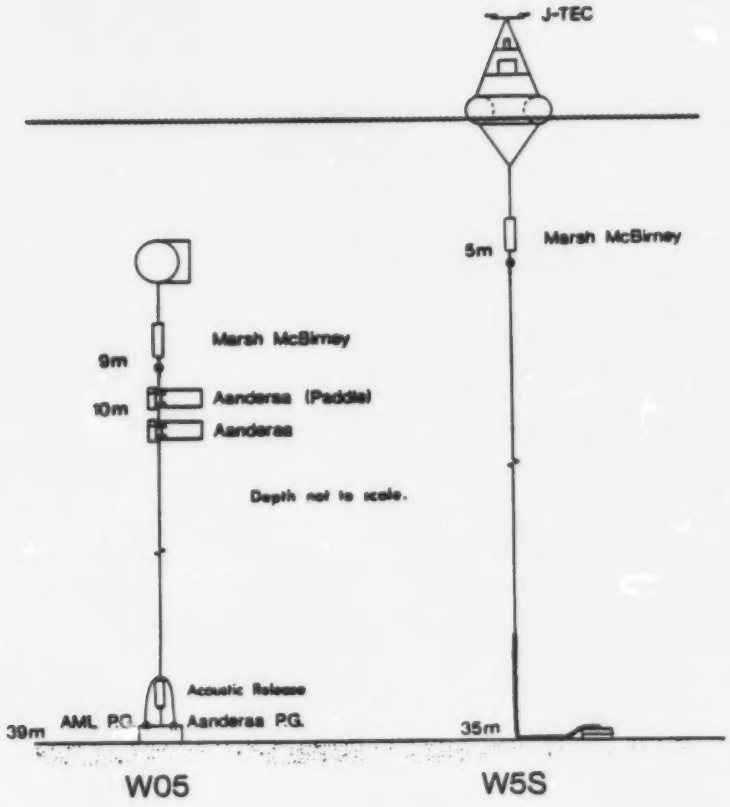

Figure 7. Moorings in Hecate Strait.

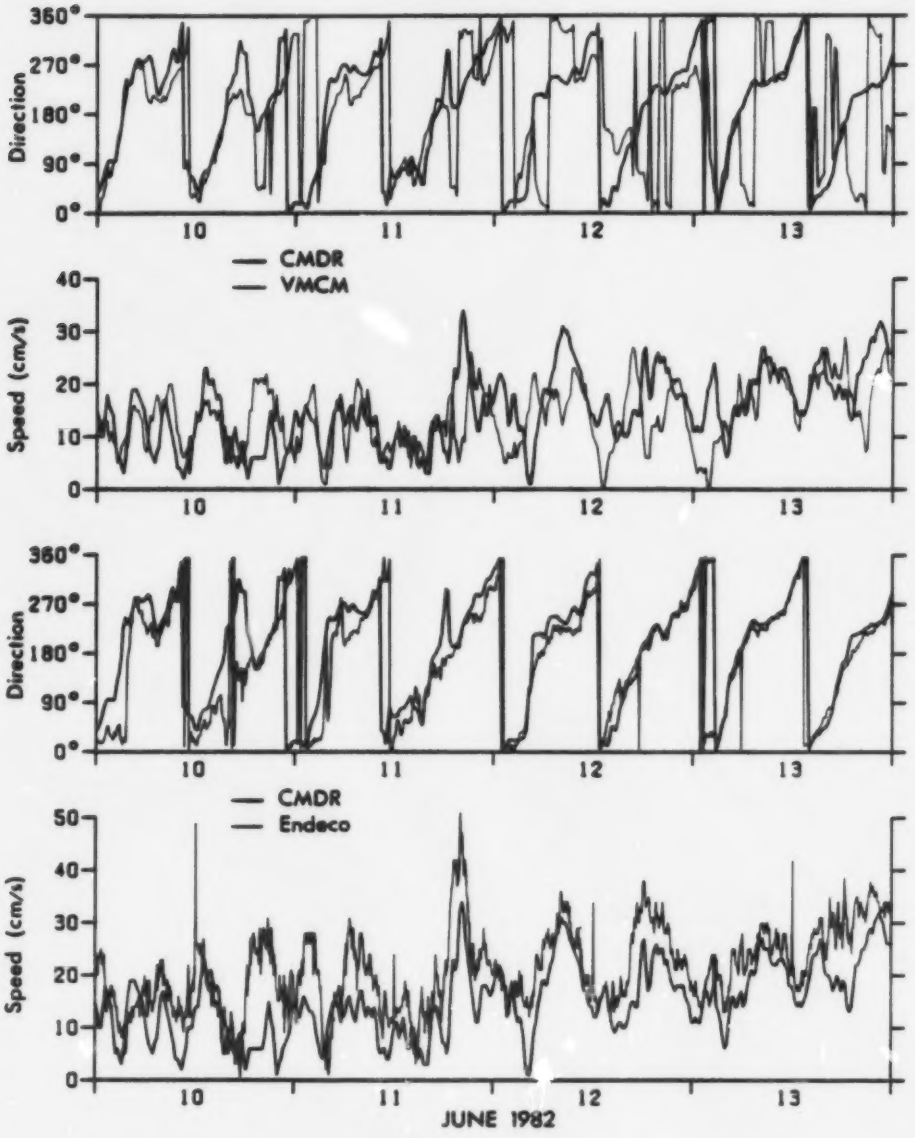

Figure 8. Time series plots of unfiltered current measurements from Queen Charlotte Sound.

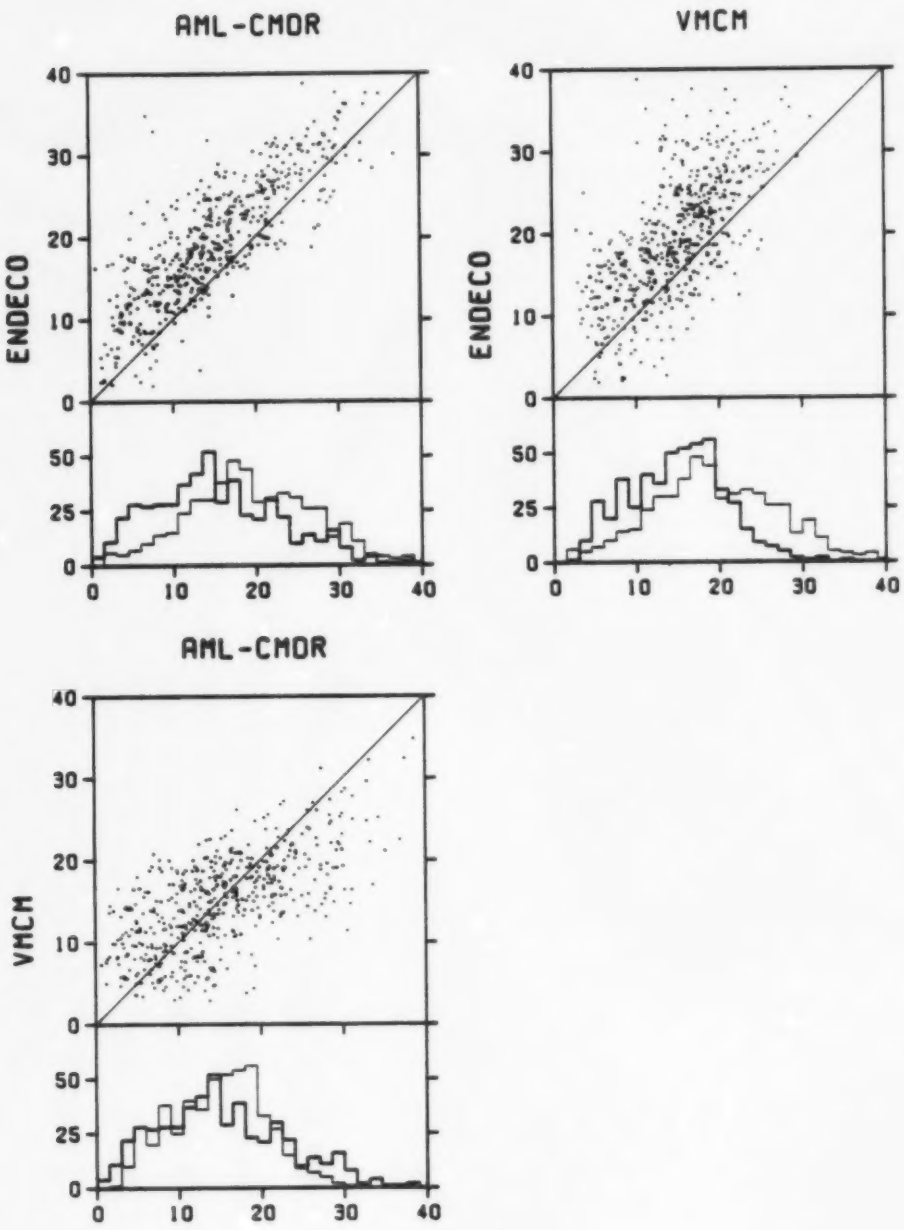

Figure 9. Scatter diagrams of speed between current meters and histograms of the occurrence of speed for Queen Charlotte Sound. The bold trace in each histogram corresponds to the speeds plotted on the horizontal axis of the attached scatter diagram.

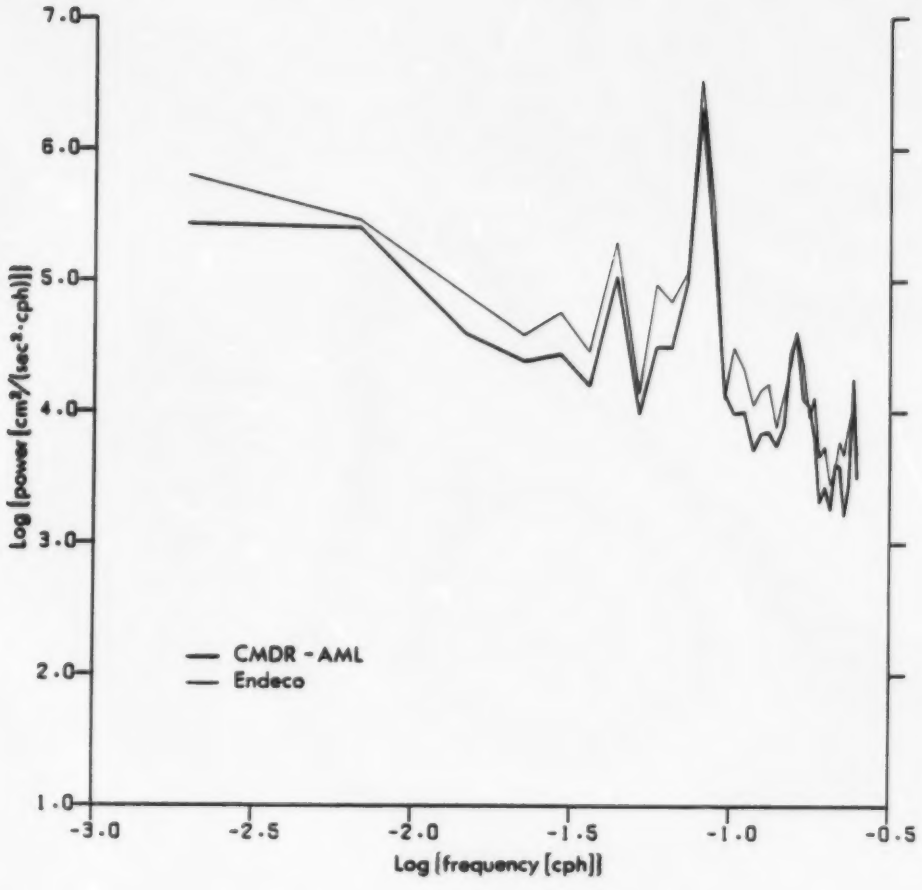

Figure 10. Power spectra of current measurements in Queen Charlotte Sound.

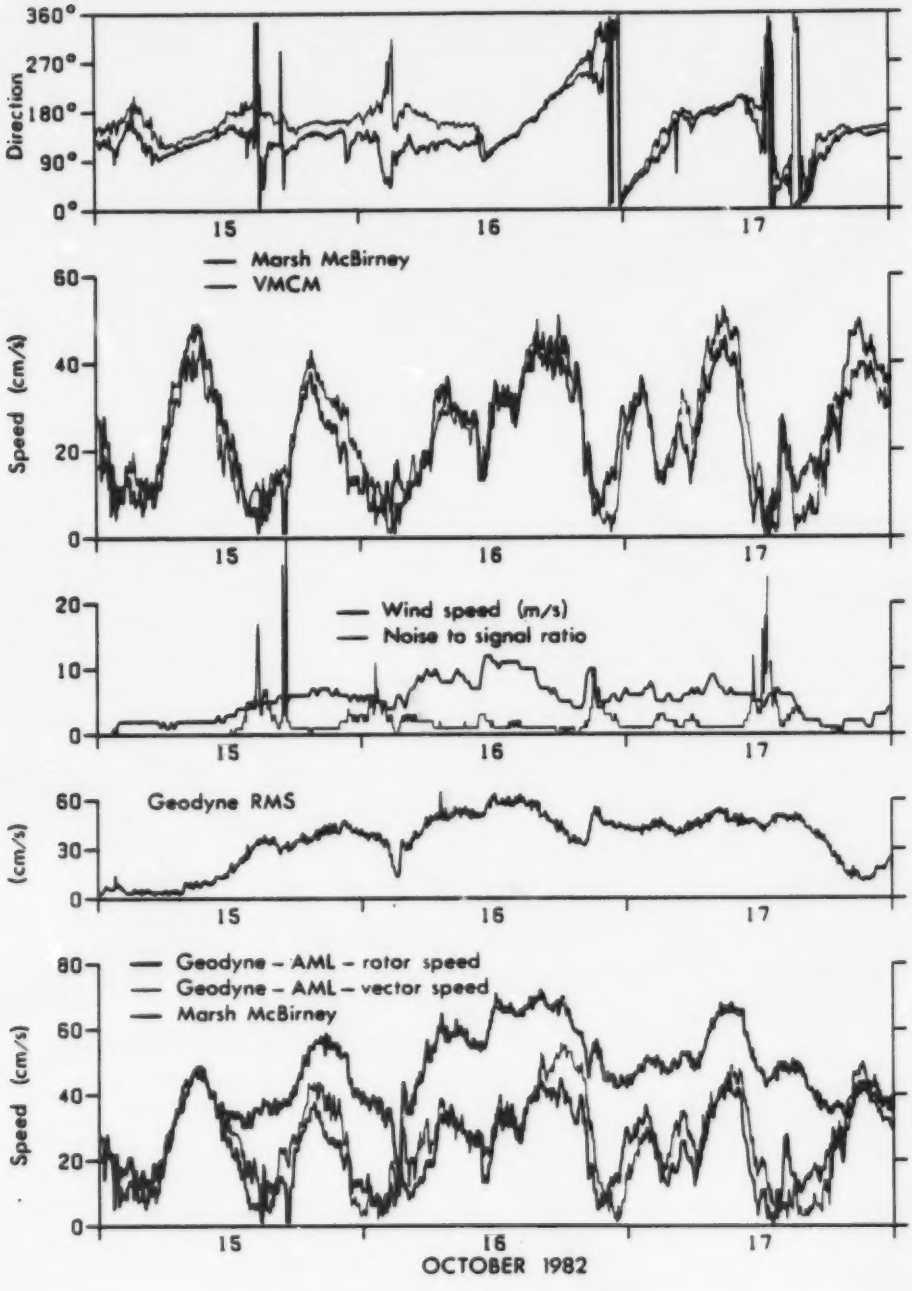

Figure 11. Time series plots of unfiltered current measurements from the surface-following mooring GMA for the period October 15-17 in the Strait of Georgia.

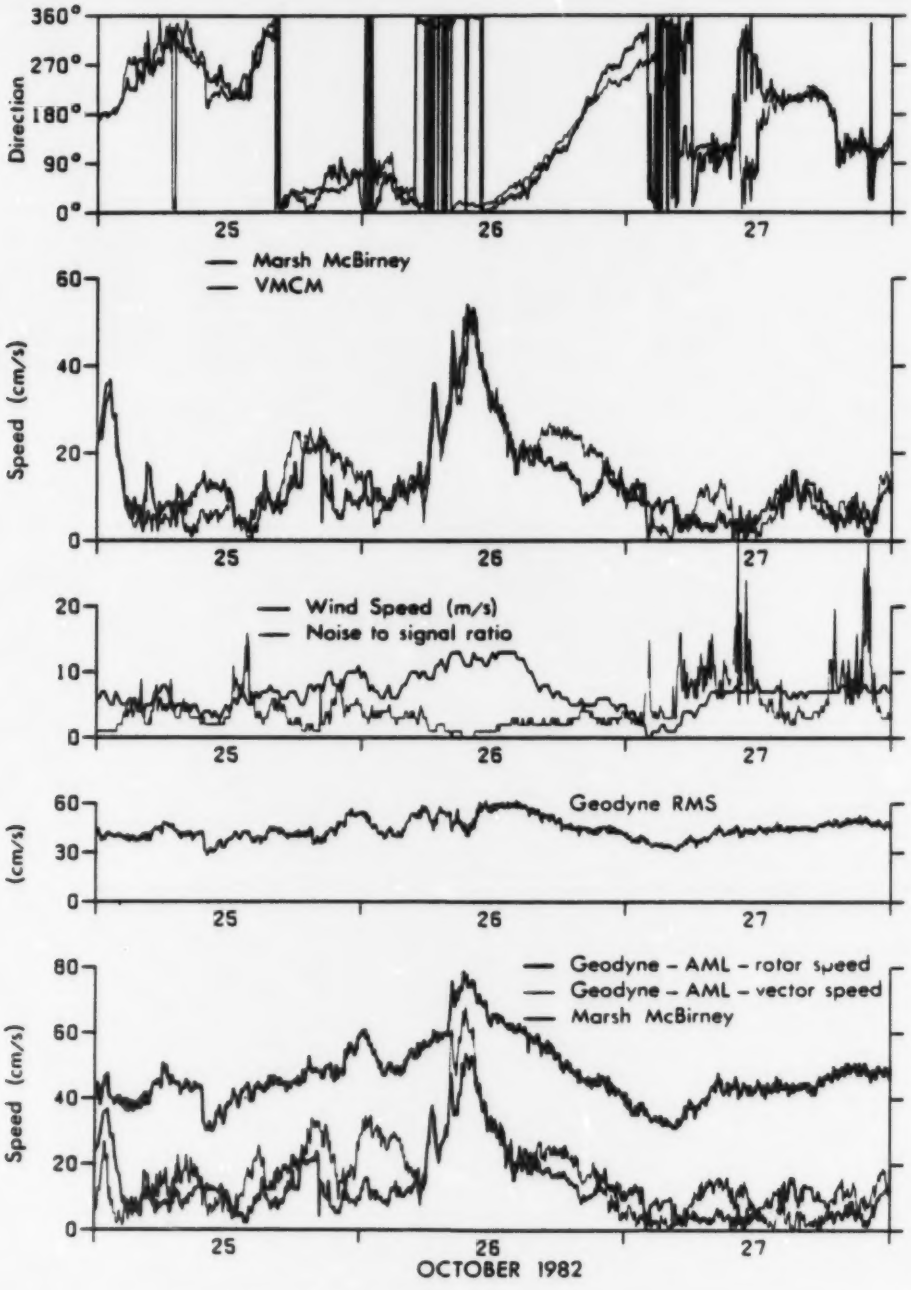

Figure 12. Time series plots of unfiltered current measurements from the surface-following mooring GMA for the period October 25-27 in the Strait of Georgia.

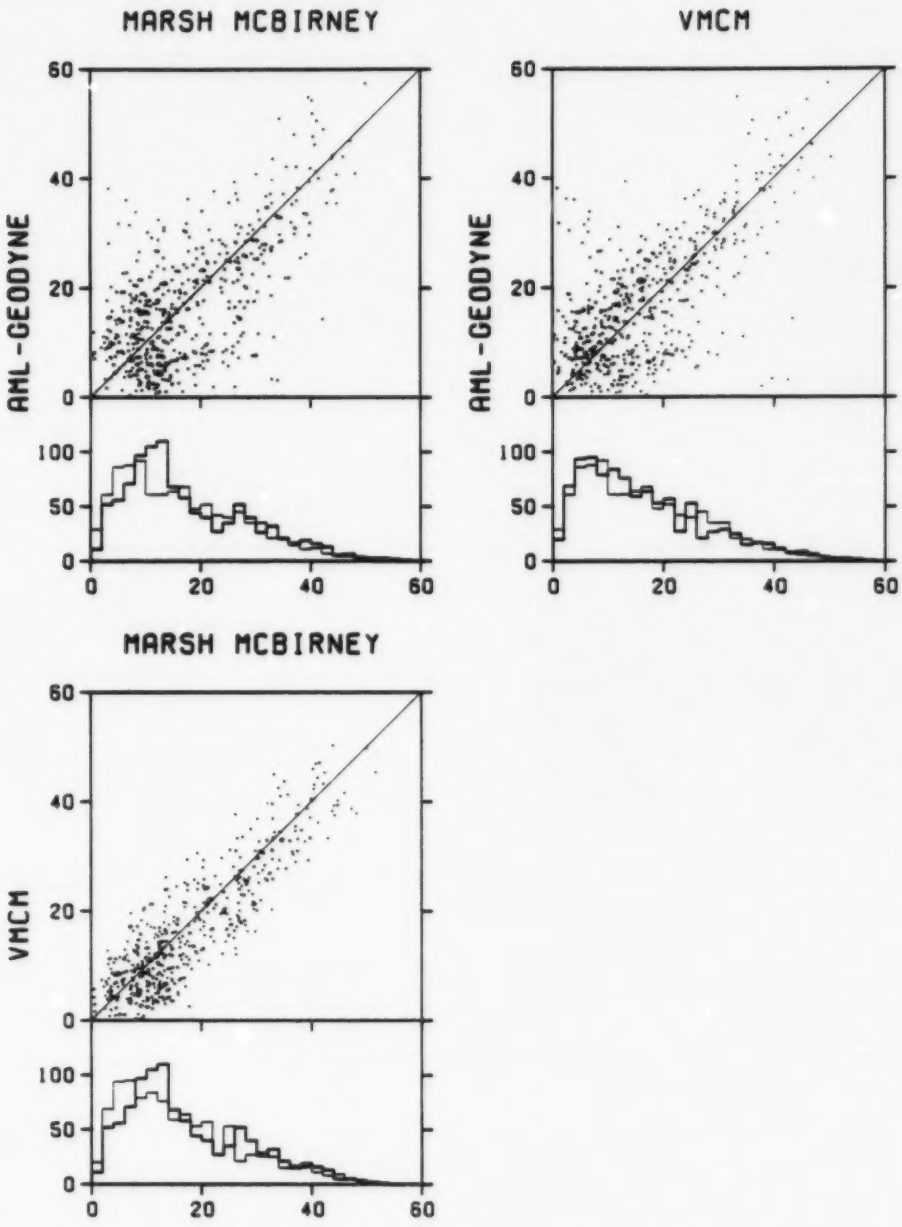

Figure 13. Scatter diagrams of speed between current meters and histograms of the occurrence of speed for the surface-following mooring GMA in the Strait of Georgia. The bold trace in each histogram corresponds to the speeds plotted on the horizontal axis of the attached scatter diagram.

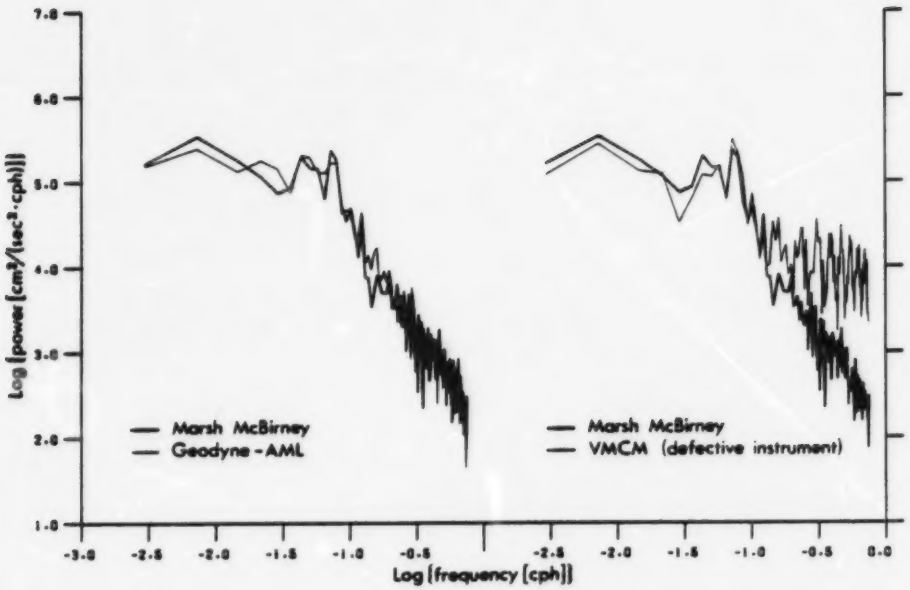

Figure 14. Power spectra of current measurements for the surface-following mooring GMA in the Strait of Georgia.

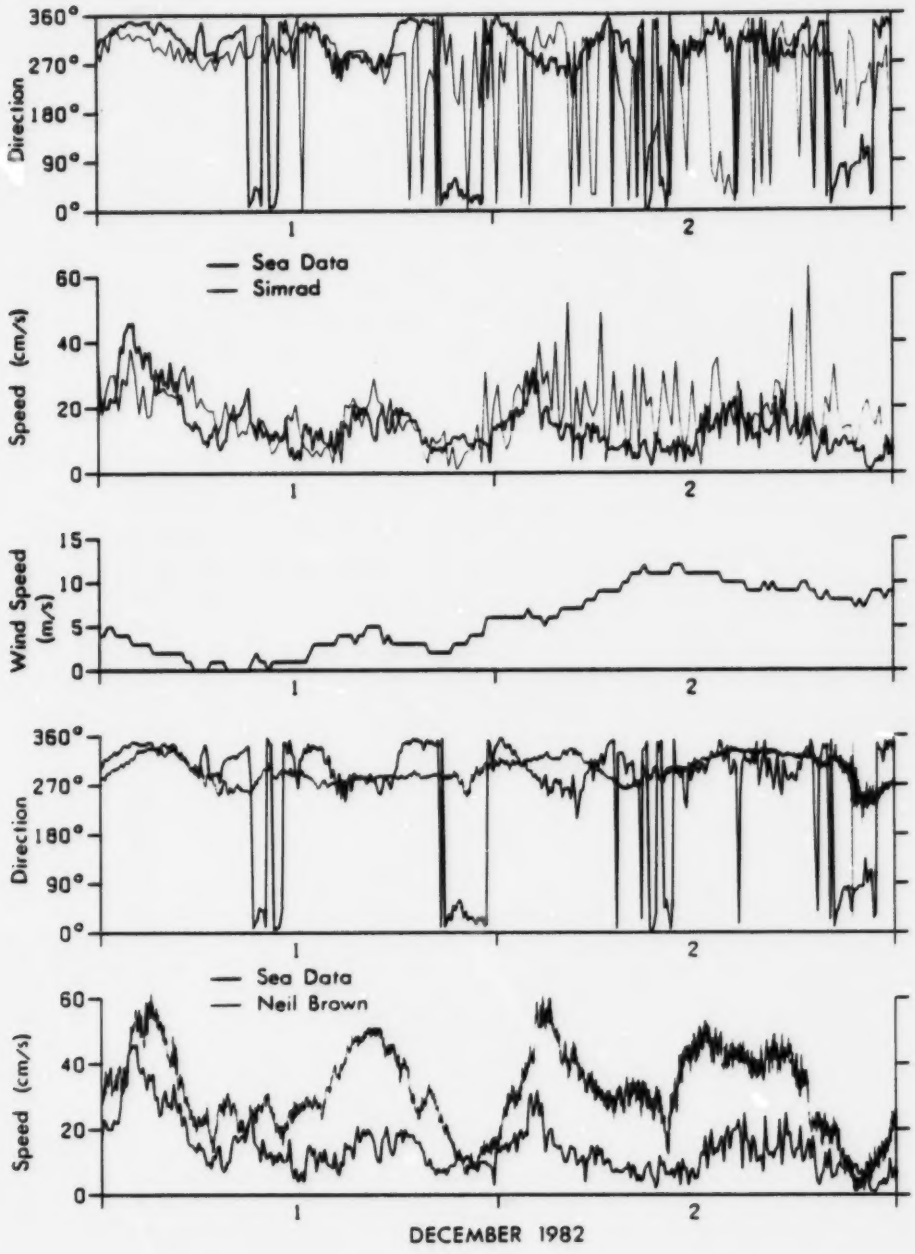

Figure 15. Time series plots of unfiltered current measurements from the surface-following mooring GMB in the Strait of Georgia.

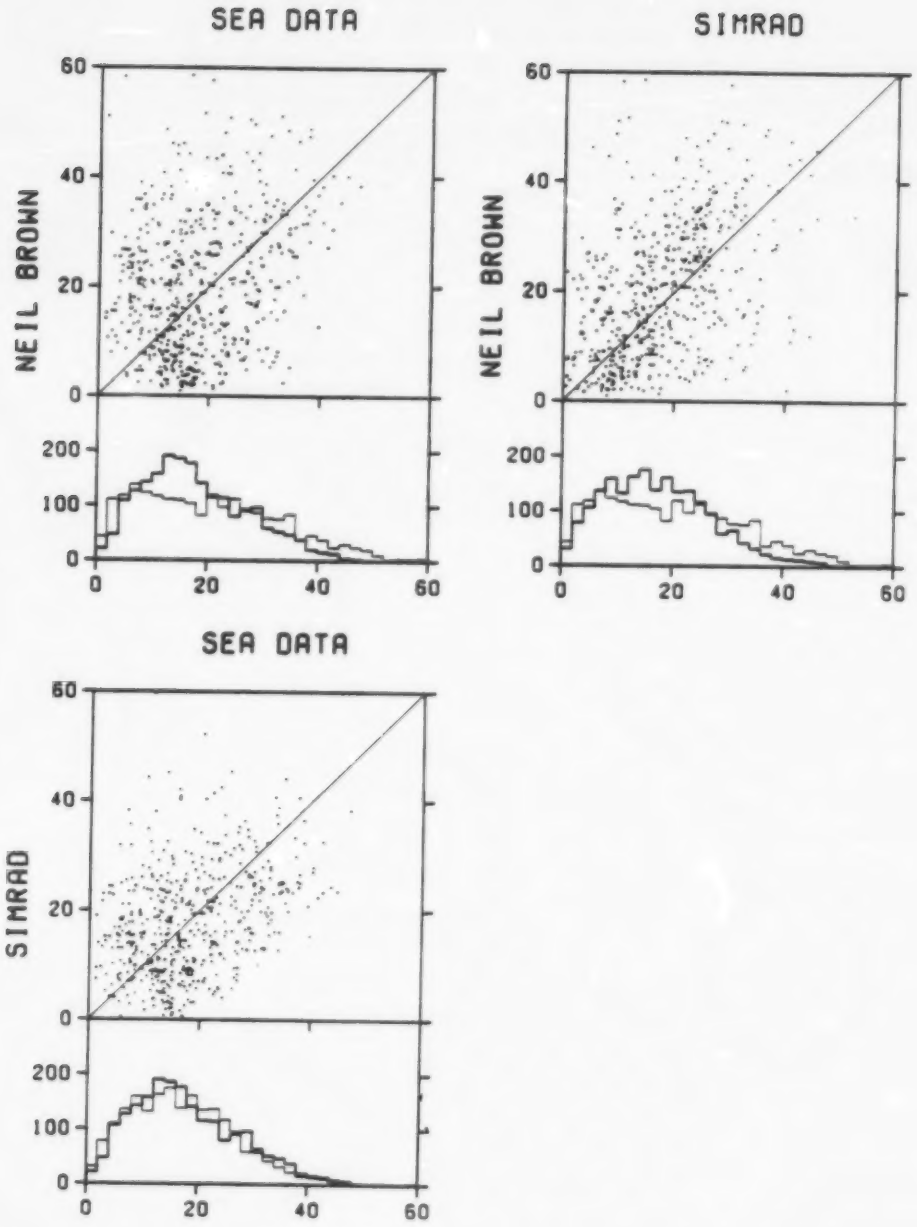

Figure 16. Scatter diagrams of speed between current meters and histograms of the occurrence of speed for the surface-following mooring GMB in the Strait of Georgia. The bold trace in each histogram corresponds to the speeds plotted on the horizontal axis of the attached scatter diagram.

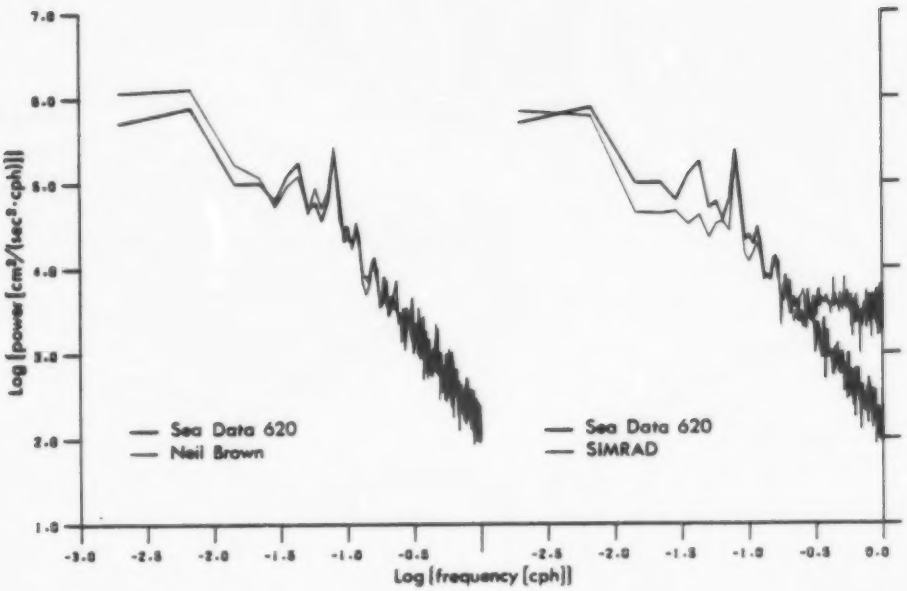

Figure 17. Power spectra of current measurements for the surface-following mooring GMB in the Strait of Georgia.

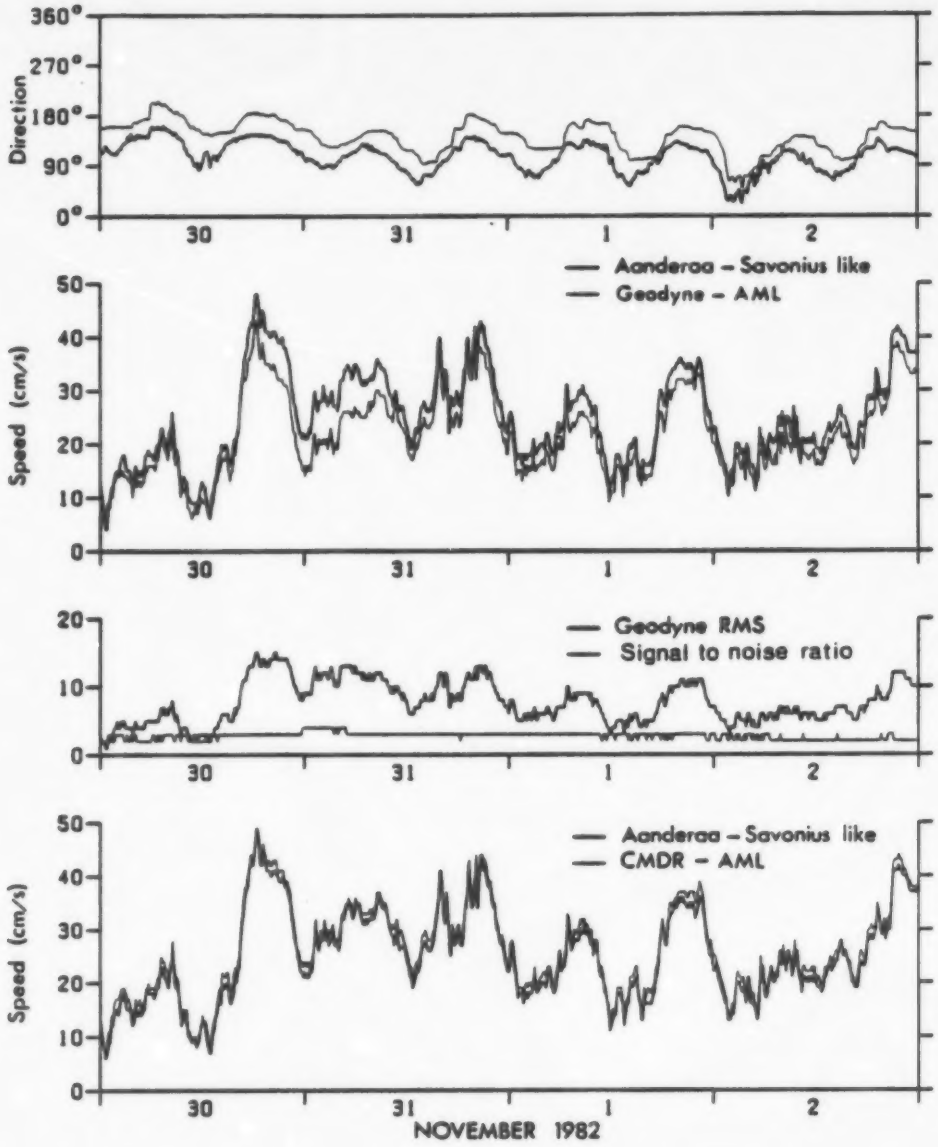

Figure 18. Time series plots of unfiltered current measurements from the instruments at 50m on the subsurface mooring GSW in the Strait of Georgia.

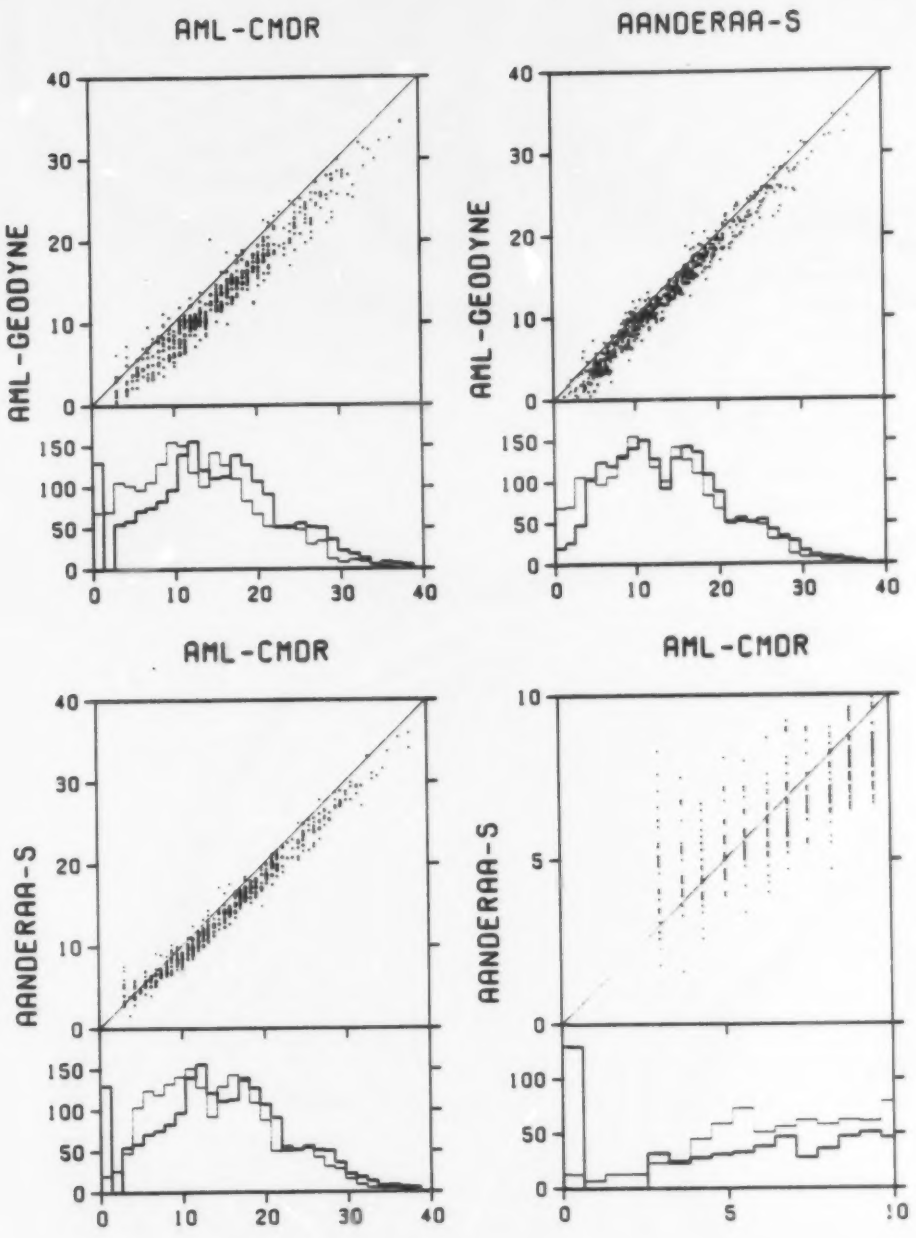

Figure 19. Scatter diagrams of speed between current meters and histograms of the occurrence of speed for the instruments at 50m on the subsurface mooring GSW in the Strait of Georgia. The bold trace in each histogram corresponds to the speeds plotted on the horizontal axis of the attached scatter diagram.

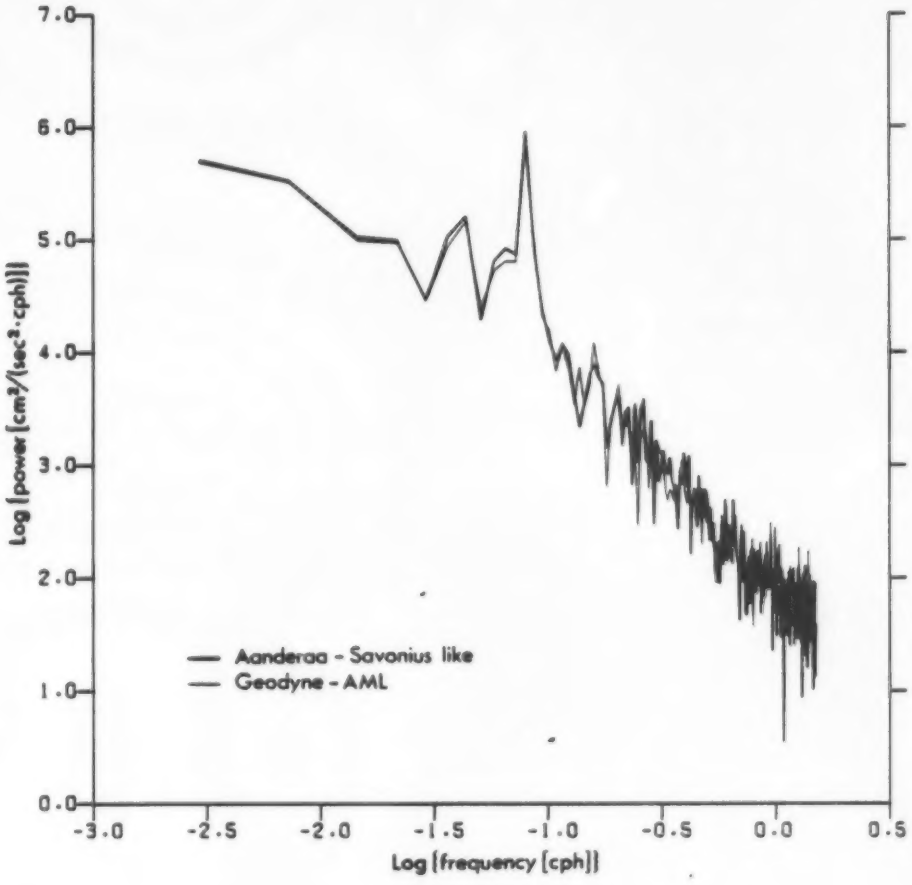

Figure 20. Power spectra of currents as measured by the Aanderaa RCM4 (Savonius-like) and Geodyne-AML instruments at 50m on the subsurface mooring GSW in the Strait of Georgia.

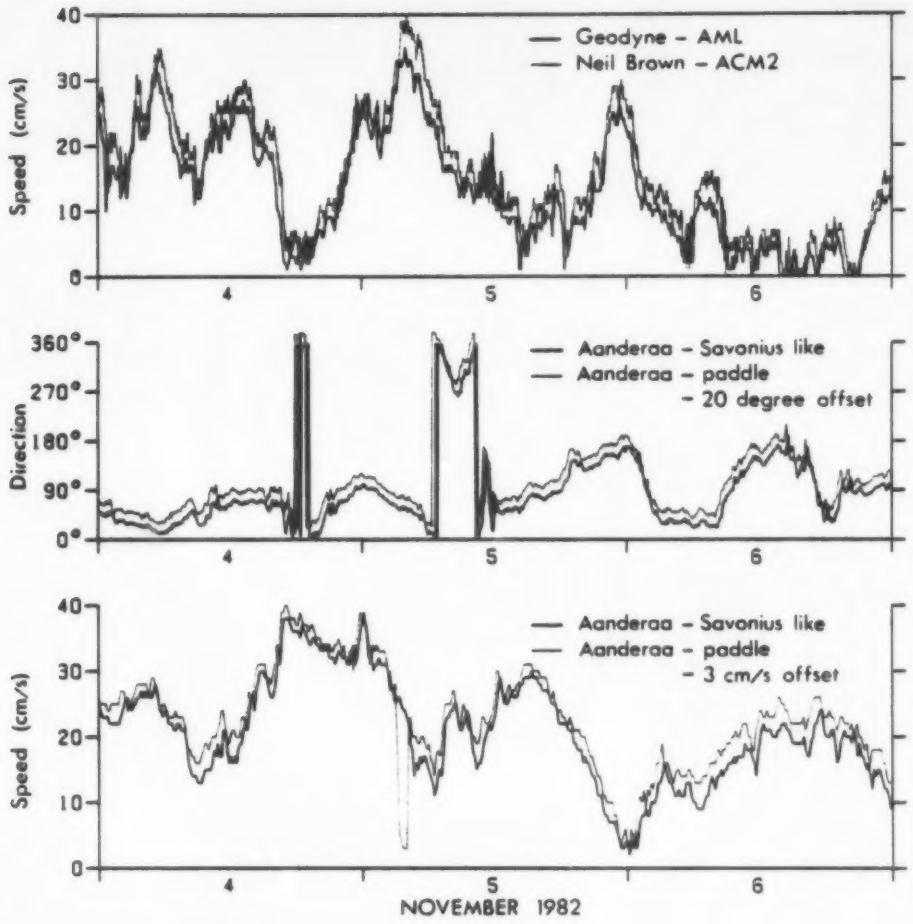

Figure 21. Time series plots of unfiltered current measurements from the instruments at 50m and 100m on the subsurface mooring GNE in the Strait of Georgia.

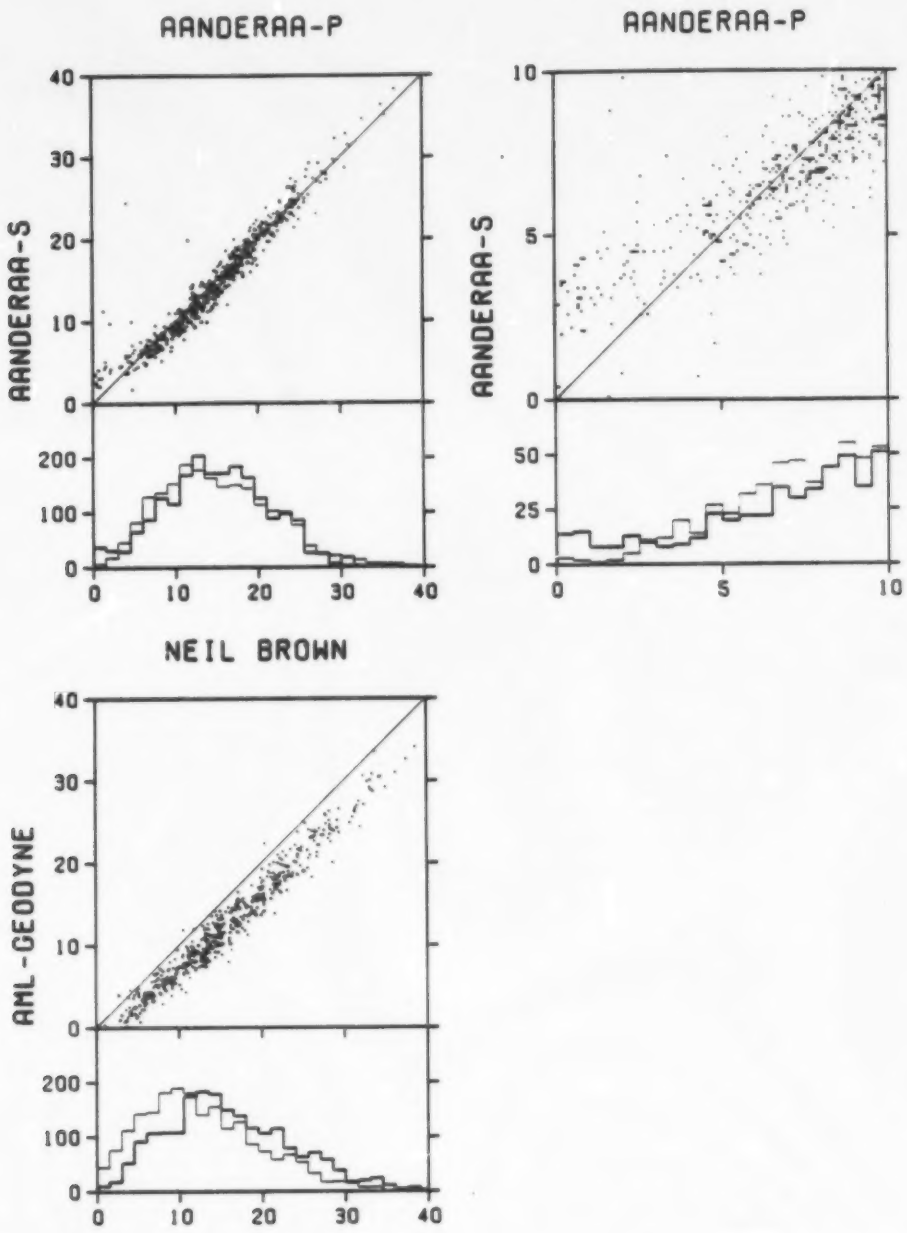

Figure 22. Scatter diagrams of speed between current meters and histograms of the occurrence of speed for the instruments at 50m and 100m on the subsurface mooring GNE in the Strait of Georgia. The bold trace in each histogram corresponds to the speeds plotted on the horizontal axis of the attached scatter diagram.

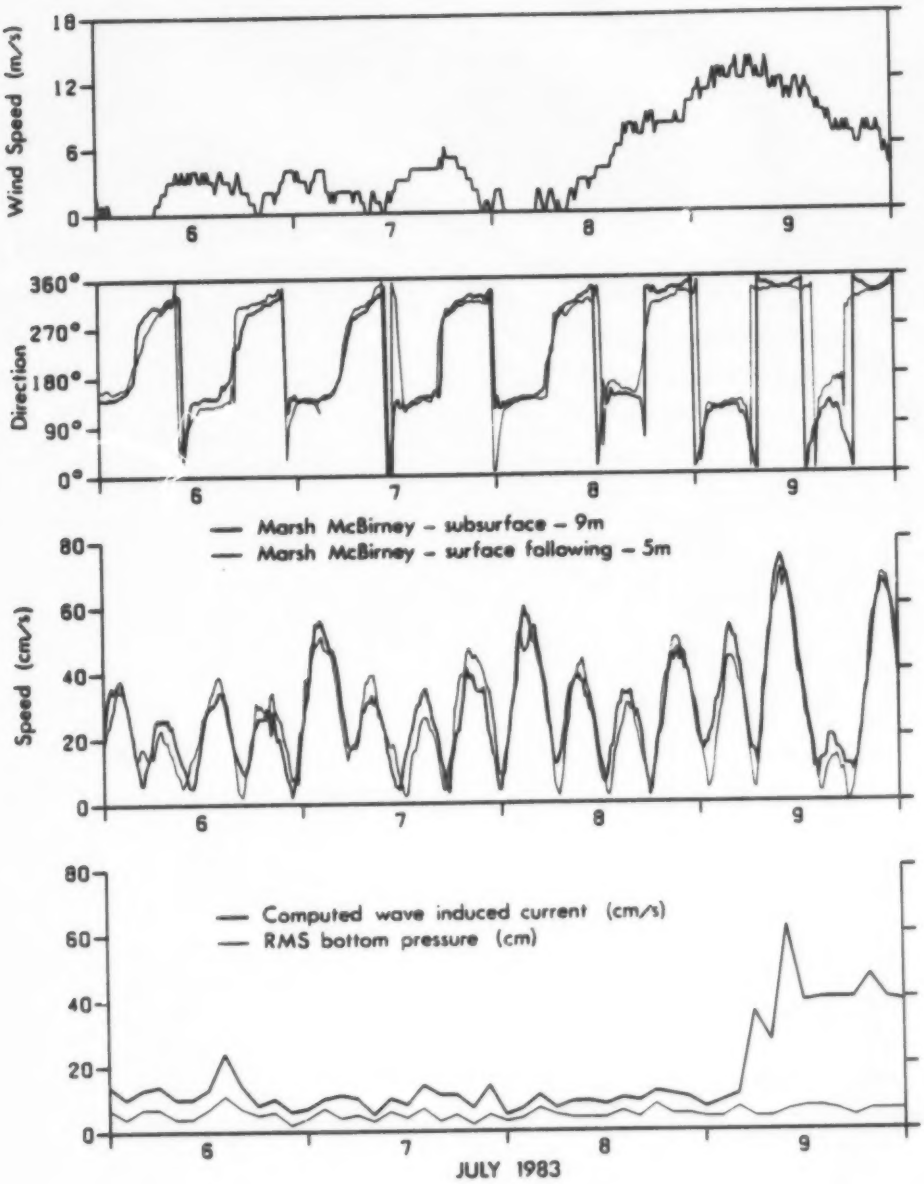

Figure 23. Time series plots of current as measured by Marsh-McBirney 585's on surface-following and subsurface moorings, W05 and W5S, in Hecate Strait.

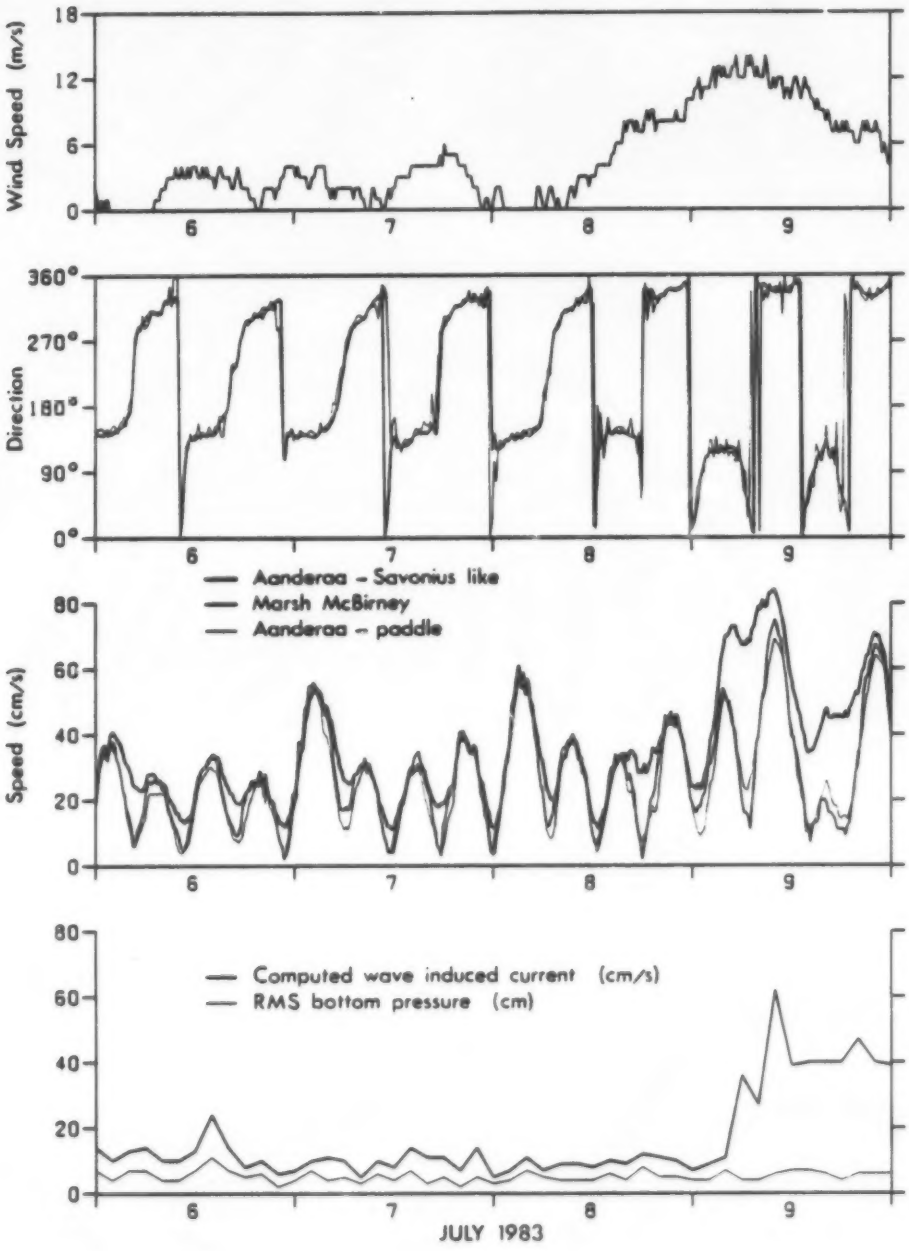

Figure 24. Time series plots of unfiltered current measurements from the subsurface mooring W05 in Hecate Strait.

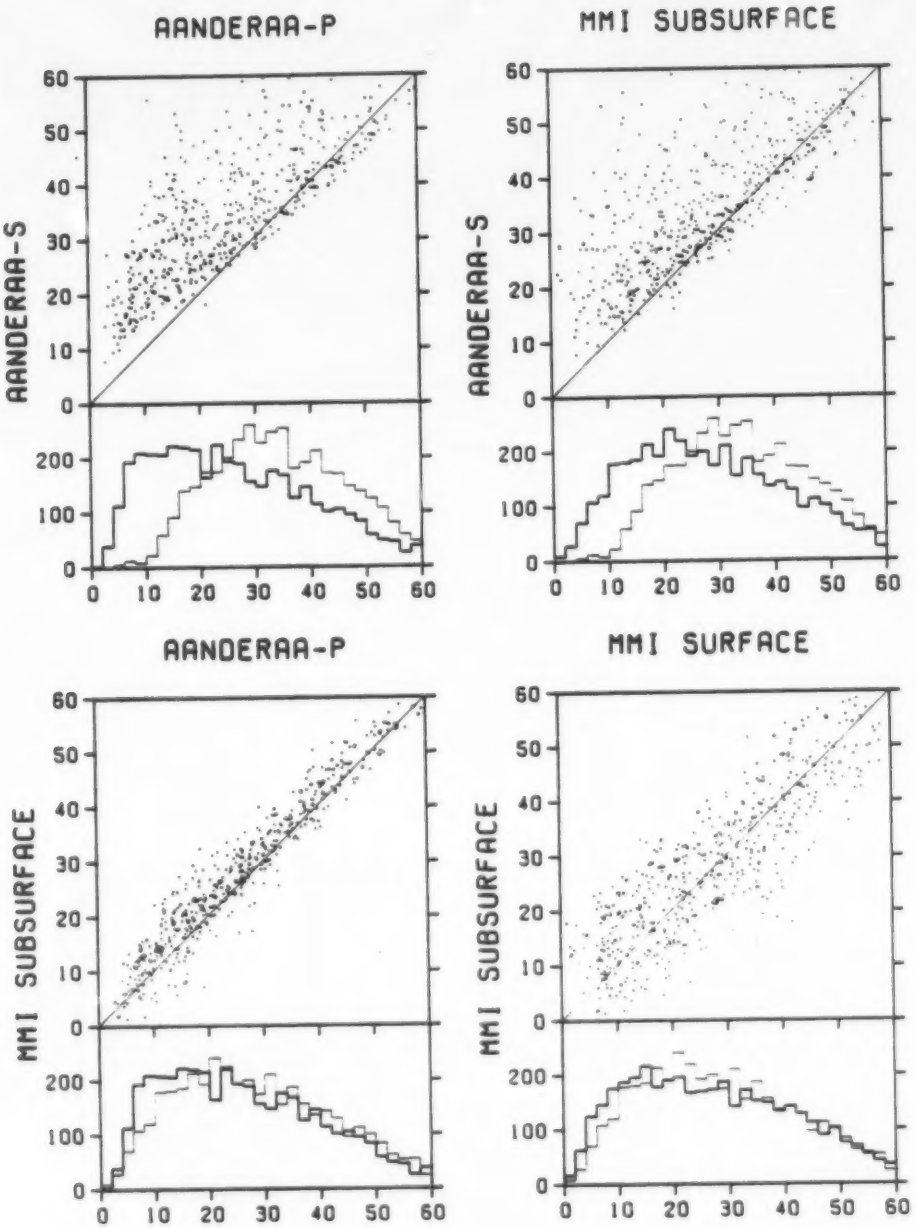

Figure 25. Scatter diagrams of speed between current meters and histograms of the occurrence of speed for Hecate Strait. The bold trace in each histogram corresponds to the speeds plotted on the horizontal axis of the attached scatter diagram.

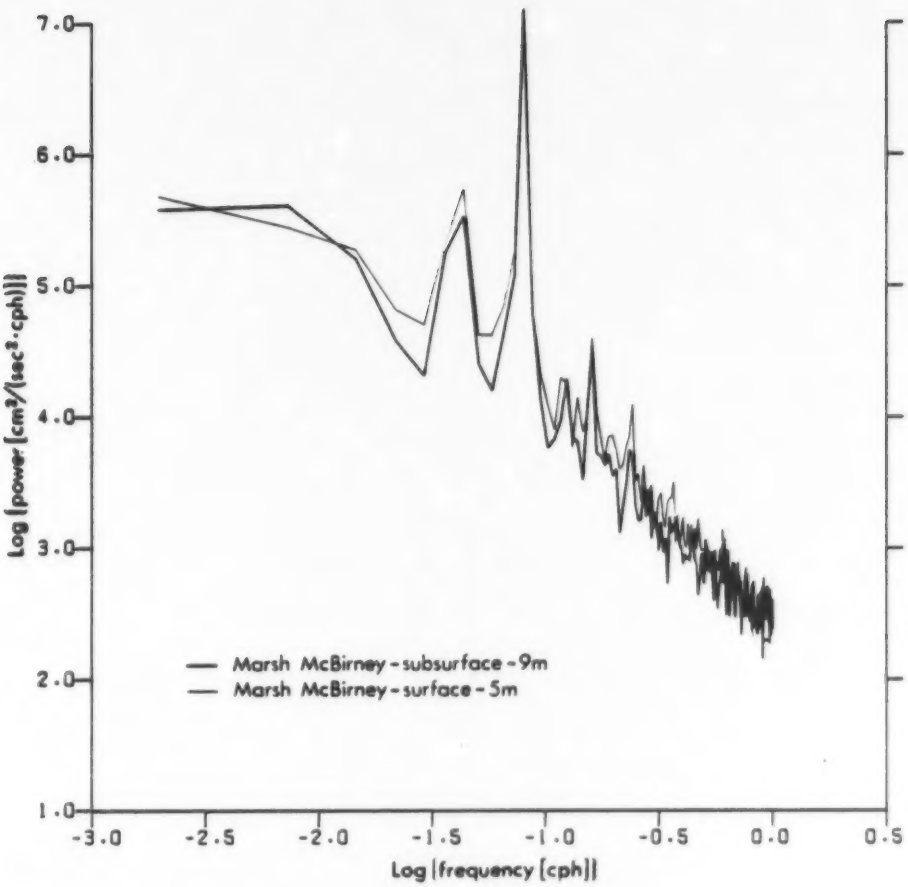

Figure 26. Power spectra of currents as measured by Marsh-McBirney 585's on surface-following and subsurface moorings, W05 and W5S, in Hecate Strait.

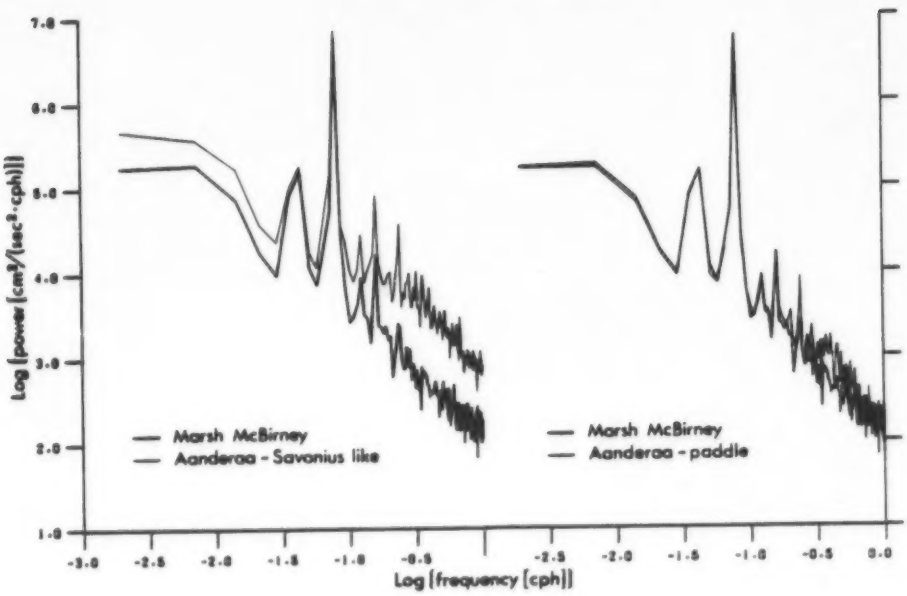

Figure 27. Power spectra of current measurements from the subsurface mooring W05 in Hecate Strait.